UNIVERSITY OF CALIFORNIA, SAN DIEGO

Silicon Nanopatterning for Device Applications

A dissertation submitted in partial satisfaction of the

requirements for the degree Doctor of Philosophy

in

Materials Science and Engineering

by

Young Oh

Committee in Charge:

Professor Sungho Jin, Chair
Professor Prabhakar Bandaru
Professor Jennifer Cha
Professor Renkun Chen
Professor Yu Qiao

2012

The dissertation of Young Oh is approved, and it is acceptable in quality and form for publication on microfilm and electronically:

Chair

University of California, San Diego

2012

Dedicated to my loving wife Jihye and my family

who have shown continuous love and concern

Today, which was proved to be fruitless,

is the day that the dead in the past was longing for.

Romain Rolland

TABLE OF CONTENTS

LIST OF FIGURES

ACKNOWLEDGEMENTS

I wish to acknowledge and deeply thank my advisors, Professor Sungho Jin for his strong encouragement, support, and guidance during the course of this research. I wish to express my gratefulness to my committee members for their time and helpful suggestions: Professor Prabhakar Bandaru, Professor Jennifer Cha, Professor Renkun Chen, and Professor Yu Qiao.

I would also like to recognize and thank the following individuals for their assistance in various aspects of this work: Dr. Chulmin Choi, Dr. Daehoon Hong, Dr. Leon Chen, Dr. Jinyeol Kim, Dr. Kunbae Noh, Dr. Yeoungchin Yoon, Prof. Seunghan Oh, Hyunsu Kim, Taekyoung Kim, Duyoung Choi, Cihan Kuru, Dr. Seongdeok Kong, and Youngjin Kim. I appreciate all the helps from my collaborators. We have shared the joy and frustration together solving countless materials, fabrications and device problems in the past several years.

I wish to thank Nano3 staffs at UC San Diego: Dr. Bernd Fruhberger, Larry Grissom, Ryan Anderson, Dr. Maribel Montero, and Sean Parks. They have been always ready to help with the nanofabrication and characterization processes.

I would truly like to thank my wonderful friends who are like family and made this incredible journey possible: Dr. Sungsik Hur, Dr. Yongsung Hwang, Prof. Soonkook Hong, Dr. Sungwhan Cho, and Dr. Jinwoo Lee for their friendship.

Special thanks go to Charlotte Lauve, Betty Manoulian, and Iris Villanueva for taking care of the administrative burdens for me.

Lastly, I wish to express my deepest gratitude to my wife, my lovely daughters (Seungyoon Oh and Ava Oh), and other family members. Thanks again to my wife, Jihye Choi, for her best support for my effort toward the PhD degree.

I also wish to thank my many friends and other colleagues who are too numerous to mention all by name.

Chapter 2, in full, has been prepared for a manuscript for publication, "Magnetically Guided Nano-Micro Shaping and Slicing of Silicon", Young Oh, Chulmin Choi, Daehoon Hong, Seongdeok Kong, and Sungho Jin. The dissertation author was the primary investigator and author of this paper.

Chapter 3, in full, is a reprint of it appear the material as s in Journal of Vacuum Science and Technology B 29, 06FD03 (2011), "Multi-tip AFM lithography system for high throughput nano-patterning", Young Oh, Chulmin Choi, Kunbae Noh, Diana Villwock, Gwangmin Kwon, Haiwon Lee, and Sungho Jin. The dissertation author was the primary investigator and author of this paper.

Young Oh

La Jolla, December 2011

VITA

1998 Bachelor of Science in Chemistry,
Hanyang University, Seoul, South Korea

2000 Master of Science in Chemistry,
Hanyang University, Seoul, South Korea

2007 Senior Research Engineer of Samsung Cheil Industries
Optical Materials Research Institute, South Korea

2012 Doctor of Philosophy in Materials Science and Engineering,
University of California, San Diego

PUBLICATIONS

Journals Articles:

[1] Magnetically Guided Nano-Micro Shaping and Slicing of Silicon, Young Oh, Chulmin Choi, Daehoon Hong, Seongdeok Kong, and Sungho Jin (in review)

[2] Multi-tip AFM lithography system for high throughput nano-patterning, Young Oh, Chulmin Choi, Kunbae Noh, Diana Villwock, Gwangmin Kwon, Haiwon Lee, and Sungho Jin, Journal of Vacuum Science and Technology B **29,** 06FD03 (2011).

[3] Di-block Copolymer Directed Anodization of Hexagonally Ordered Nanoporous Aluminum Oxide, Kunbae Noh, Chulmin Choi, Hyunsu Kim, Young Oh, Jin-Yeol Kim, Se-Yeon Jeong, Tae-Yeon Seong, and Sungho Jin, Journal of Vacuum Science and Technology B **29,** 06F207 (2011).

[4] Fabrication and magnetic properties of nonmagnetic ion implanted magnetic recording films for bit-patterned media, Chulmin Choi, Kunbae Noh, Young Oh, Daehoon Hong, Leon Chen, and Sungho Jin, IEEE Trans. Mag. **47(10)**, 2532 (2011).

[5] Diameter-reduced islands for nanofabrication toward bit patterned magnetic media, Chulmin Choi, Kunbae Noh, Young Oh, Cihan Kuru, Daehoon Hong, Villwock, D., Li-Han Chen, and Sungho Jin, IEEE Trans. Mag. **47(10)**, 2536 (2011).

[6] Magnetic Properties of Antidot Patterned Co/Pd Multilayer Film, Kunbae Noh, Chulmin Choi, Hyunsu Kim, Young Oh, Jin-Yeol Kim, Daehoon Hong, Li-Han Chen, and Sungho Jin, IEEE Trans. Mag. **47(10)**, 3478 (2011).

[7] Planarization of patterned magnetic recording media to enable head flyability, Chulmin Choi, Yeoungchin Yoon, Daehoon Hong, Young Oh, Talke, F.E., and Sungho Jin, Microsystem Technologies **17(3)**, 395 (2011).

[8] Long-Range Ordered Aluminum Oxide Nanotubes by Nanoimprint-Assisted Aluminum Film Surface Engineering, Kunbae Noh, Chulmin Choi, Jin-Yeol Kim, Young Oh, Karla Brammer, Mariana Loya, and Sungho Jin, Journal of Vacuum Science and Technology B **28(6)**, C6M88 (2010).

[9] Enhanced Magnetic Properties of Bit Patterned Magnetic Recording Media by Trench-Filled Nanostructure, Chulmin Choi, Daehoon Hong, Young Oh, Kunbae Noh, Jin Yeol Kim, Leon Chen, Sy-Hwang Liou, and Sungho Jin, Electronic Materials Letters **6(3)**, 113 (2010).

[10] Strongly Superhydrophobic Silicon Nanowires by Supercritical CO_2 Drying, Chulmin Choi, Yeoungchin Yoon, Daehoon Hong, Karla S. Brammer, Kunbae Noh, Young Oh, Seunghan Oh, Frank E. Talke and Sungho Jin, Electronic Materials Letters **6(2)**, 59 (2010).

[11] Planarization of Discrete Track Recording Media to Improve Flyability of Magnetic Recording Sliders, Youngchin Yoon, Chulmin Choi, Young Oh, Daehoon Hong, Sungho Jin, and Frank E. Talke, IEEE Trans. Mag. **45(10)**, 3527 (2009).

[12] Nanopatterning of self-assembled monolayers on Si-surfaces with AFM lithography, Won Bae Lee, Young Oh, and Eung Ryul Kim, Synthetic Metals **117**, 305 (2001).

[13] Nanolithography of self-assembled zirconium N, N'-bis(ethyl dihydrogen phosphate)-3,4,9,10-perylene(dicarboximide) (EPPI) layer on silicon surface, See Hyun Kim, Young Oh, and Haiwon Lee, Molecular Crystals and Liquid Crystals **349**, 175 (2000).

[14] Atomic force microscope lithography with octadecyldimethyl-methoxysilane monolayer resists, Young Oh, Jinchul Kim, and Haiwon Lee, Molecular Crystals and Liquid Crystals **337**, 7 (1999).

[15] Atomic force microscope lithography with organosilane resists, Young Oh, Jinchul Kim, and Haiwon Lee, Journal of the Korean physical society **35**, S1013 (1999).

[16] Atomic force microscope based nanolithography of self-assembled organosilane monolayer resists, Jinchul Kim, Young Oh, and Haiwon Lee, Japanese Journal of Applied Physics **37(12B)**, 7148 (1998).

Patents:

[1] Article Comprising Thin Sliced Semiconductors by Magnetic-Field-Guided Etching, Method of Slicing, and Device Applications, UCSD Docket No. SD2010-071

[2] Ultra-High-Density, High-Throughput, Nanopatterns by Localized Oxidation using Electric Field Activated Array Nanoprobes, and Methods and Applications, UCSD Docket No. SD2009-043

ABSTRACT OF THE DISSERTATION

Silicon Nanopatterning for Device Applications

by

Young Oh

Doctor of Philosophy in Materials Science and Engineering

University of California, San Diego, 2012

Professor Sungho Jin, Chair

At least 90% of current photo-voltaic (PV) solar cells are dominated by silicon based structures. For practical use, silicon needs to be physically processed by slicing into wafers and polished, and microscale / nanoscale geometrical changes added for circuits and devices. After the wire sawing procedure, less than 50% of the silicon feedstock ends up as useful wafers with the remaining Si material lost as sawing slurry (kerf loss). Since approximately one-half of the cost of the high-efficiency, crystalline Si solar cells is the silicon materials cost, it would be highly desirable to reduce the slicing loss and usage of Si in the solar cells.

In view of the expanding needs for thin Si for variety of applications such a flexible, bendable or stretchable electronics, nanowire shaped Si for advanced PV solar

cells as well as a need to produce affordable PV solar cells with substantially reduced Si materials cost, convenient direction-controllable and rapid Si shaping technique is highly desirable. We have created here a new and unique Si slicing and patterned shaping method using magnetically direction-guided etching. The method can produce very thin Si sheets or create zig-zag Si wires, with a possibility of obtaining Si wafers essentially ignoring the crystallographic preferred etch directions. The application of magnetic force and gradient field accelerates the kinetics of Si etching/slicing. The Si slicing waste during the magnetically guided slicing can be minimized to be as small as 5 μm or less thickness per each Si slicing, as compared to at least an order of magnitude more loss for common mechanical slicing. These studies are discussed in chapter 2.

We also described nanopatterning techniques using atomic force microscopy (AFM) based or nano-manipulator based patterning of a substrate surface using localized oxidation of nano-islands or localized changes of surface structure due to applied voltage through the tip of multi-probe. Some embodiments include the utilization of an arrayed nanoprobe for simultaneous writing of many islands or lines, followed by a pattern transfer by reactive ion etching. These studies are discussed in chapter 3.

CHAPTER 1: Introduction

1.1 Motivation and Background

1.1.1 Silicon manufacturing

Silicon geometry typically can need to be physically processed and shaped by processes including dry etching or wet etching before it can be used in devices or circuits. Physical processing can involve cutting, grinding and blade dicing, or patterning for formation of specifically designed lines, grooves, pores or vertical columns. The problem with conventional slicing technique is that silicon could easily be mechanically damaged, the slicing throughput is relatively low, e.g., with saw blade or laser cutting, and that a significant amount of silicon could be naturally discarded during the process, for example, by cutting with a blade having a finite thickness. These problems lower productivity and raise device cost. A dry etching (or reactive ion etching), which can produce a certain pattern or array on silicon, can be performed in parallel fashion using photolithography masking, but this is a rather slow and expensive processing. Wet etching is relatively simpler and cheaper but a well controlled etching and slicing of silicon at a desired speed is often difficult.

At least 90% of current photo-voltaic (PV) solar cells are dominated by silicon material. For practical use, silicon needs to be physically processed, for example, by slicing into wafers and microscale / nanoscale geometrical changes for circuits and devices. After the wire sawing procedure, 45% ~ 50% of the silicon feedstock ends up in a wafer. The remaining Si material is lost in the cutting process with the main loss as

sawing slurry, which is not recoverable.

Approximately one half of the cost of the currently dominant, high efficiency solar cells based on crystalline Si wafers (typically ~200 ㎛ thick.) is the Si materials cost. For Si photo-voltaic solar cells to be a major practical factor as a world renewable energy technology, it is highly desirable to reduce the Si materials usage.

Because of the much increased demands for silicon for semiconductor devices and solar cells, the availability aind pricing of silicon material have become important practical issues, and it would be highly desirable if silicon can be sliced or patterned in a massively parallel manner for economical processing with minimal waste of material. This technology describes a new magnetically guided semiconductor slicing technique and device applications using such thin sliced semiconductors including silicon, germanium or alloys containing Si, Ge, or both. Using such a revolutionary path of Si processing can enable a significant reduction of crystalline Si materials waste and usage in PV cells by a factor of at least ~5, preferably at least ~10, which can lead to a large cost reduction of solar cells to help enable accelerated PV solar cell deployments. In the this technology, such a reduction in crystalline Si materials usage is accomplished in two ways; i) through drastically reduced saw cut materials loss, and ii) through enabling hitherto impossible, massively parallel slicing of Si to a thinner wafer, which can be as thin as 10-20 ㎛ thick.

Wet chemical, electroless etching method using a metal as a catalyst can be implemented for silicon nanowire array or porous silicon fabrication for various potential applications such as photonic, photovoltaic, solar cells, capacitors, membranes and through-wafer interconnections. The kinds of catalyst metal used can include gold, silver

and platinum and the chemical etching solutions include H_2O_2 as oxidizing agent and HF to dissolve oxide. When silicon particles were placed on a silicon substrate and they are dipped into an etchant solution including HF and H_2O_2, etching begins from the contact interface between metal particles and silicon substrate. In time, the metal particles penetrate the silicon forming pores, and a sufficient pore formation also results in vertically aligned nanowires of silicon. However, these processes can produce irregular nanowires or nanopores rather than the desired slices. The etch speed can be relatively slow, and the direction of the chemical etching sometimes deviates from the desired vertical direction.

1.1.2 Atomic force microscopy

Since the invention of the AFM, it has been applied mainly in the study of surface topography [1], friction [2], surface adhesion and deformations [3]. The AFM records interatomic forces between the apex of a tip and atoms in a sample as the tip is scanned over the surface of the sample. When the AFM is operated in a mode (contact mode) that senses the repulsive forces between tip and sample, the tip actually touches the sample. At these small tracking forces, the tip can trace over individual atoms without damaging the surface of the sample.

The AFM can also be operated so that it senses the attractive forces (non-contact mode) between the tip and the sample. The feedback system then prevents the tip from touching and damaging the sample. The tip can be made of a small fractured diamond fragment attached to a spring in the form of a cantilever. The small repulsive tracking

forces between the tip and the sample, usually in the range of 10^{-6} to 10^{-9} N, are recorded by measuring minute deflections of the cantilever. A typical spring constant for a cantilever would be about 1 N/m. Microcantilevers made of silicon oxide with silicon etching technology [4] are even lighter and have resonant frequencies as high as 100 kHz. The higher the resonant frequency, the less sensitive the cantilever is to vibrations and the more stable it is for atomic force microscopy.

Through the Figure 1-1 we can know how optical deflection system is operated in AFM. The demonstrated ability of scanning probes such as the STM to image and modify surfaces at the atomic level has generated a considerable interest in their use for the fabrication of nanostructures [5].

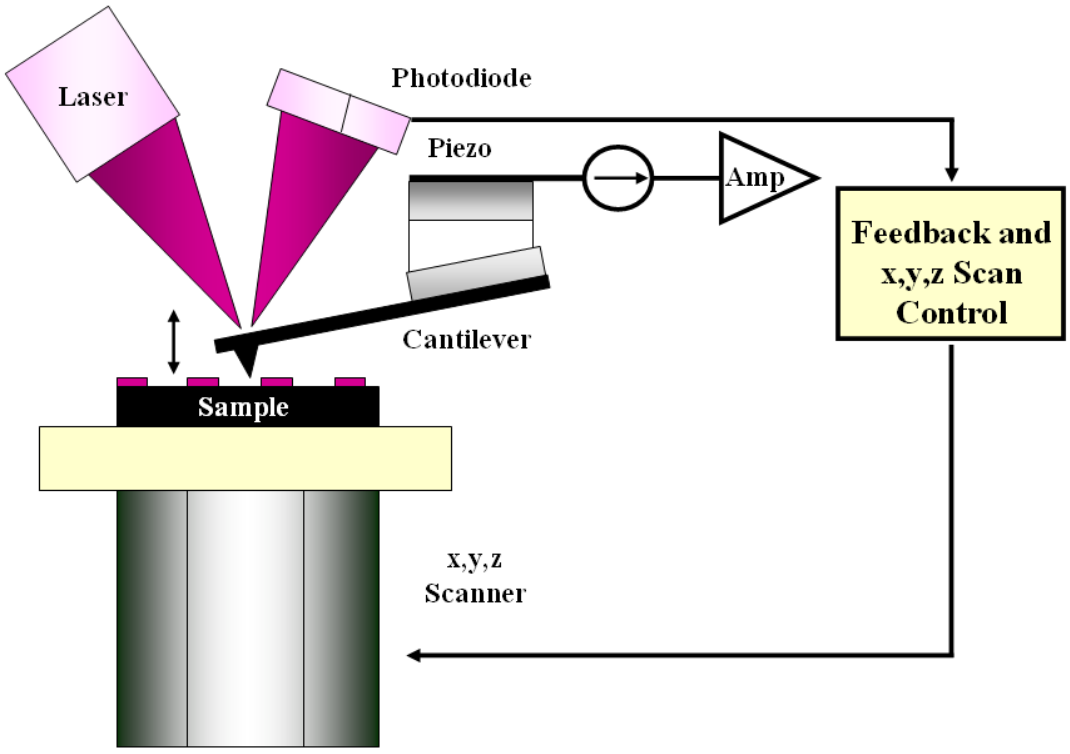

Figure 1-1. Schematic diagram of the atomic force microscopy

Recent techniques have been developed which use scanning probe microscopy (SPM) as a tool to fabricate nanometer-scale structures on ultrathin resists. Manipulation of atoms or molecules with SPM and its application to the development of novel devices or novel memory systems have been studied extensively. Scanning probe microscopy (SPM) such as the scanning tunneling microscopy (STM) and the atomic force microscopy (AFM) have been used to modify the surface on a nanometer-scale utilizing various interactions between a tip and substrate [6, 7].

For lithography, the AFM has a distinct advantage over the STM because AFM can be used for insulating as well as conducting materials. And patterning by the AFM tip can be used for nanometer scale lithography with narrower than those obtained by the use of photon [8], electron [9] and scanning probe lithography [10-13]. This decoupling of the feedback control from the exposure mechanism allows the AFM to operate on insulating as well as conducting surfaces. Despite this advantage there have been relatively few attempts at AFM-based lithography.

Resist films must be prepared in a thin and uniform layer in order to attain high spatial resolution nanometer scale. These organic molecules are spontaneously chemically bind to solid substrates such as silicon and gold. In addition to forming a highly ordered layer, resist films should be chemically resistant to many common acids and solvents and must be stable at moderately high temperature.

1.1.3 Electron emission

Appreciable electron emission occurs when a cold metal surface in a vacuum is subjected to an electron-accelerating field. This process called field emission, was first reported in 1897 by R. W. Wood and quantified using quantum mechanics by E. Fowler and L. Nordheim in 1928. Main function is to supply electrons for the generation of the electrons from a substance can be induced by application of heat (thermionic emission), strong electrical fields (high-field emission or field emission), electromagnetic radiation (photoelectric emission), or atomic particles (secondary emission). Only the field emission is used to generate the electron beam in AFM.

In the cathode, the negative electrons are held in orbits around the positive nuclei of the atoms. The strength of the positive force of the atomic nucleus holding the electrons in orbit is the greatest for those electrons next to the nucleus (K and L orbitals) and the least for those electrons farther from the atomic nucleus (M and N orbitals). The electrons in the outer orbit of the atom are the valence electrons. The valence electrons have the least holding force exerted on them by the atomic nucleus and are, therefore, the easiest electrons to remove from the atom. The electrons in the lowest orbital (K shell electrons) have the lowest energy, while those in the outer orbitals, however, do not have sufficient kinetic energy to escape from the surface of the metal.

In field emission, the potential energy curve is changed. If a strong electron-accelerating field is applied to the metal surface, there is a fall in the potential energy needed for an electron to escape. A material with low work function usually has a large atomic radius, or has a large spacing between the atoms in the crystal structure, and the rougher and cleaner the surface is, the greater the emission of electrons. The farther from

the surface of the metal, the greater is the fall in necessary energy. Field emission is substantially independent of temperature, and electron emission from the surface of the metal increases with an increase in the electron-accelerating field according to an exponential law.

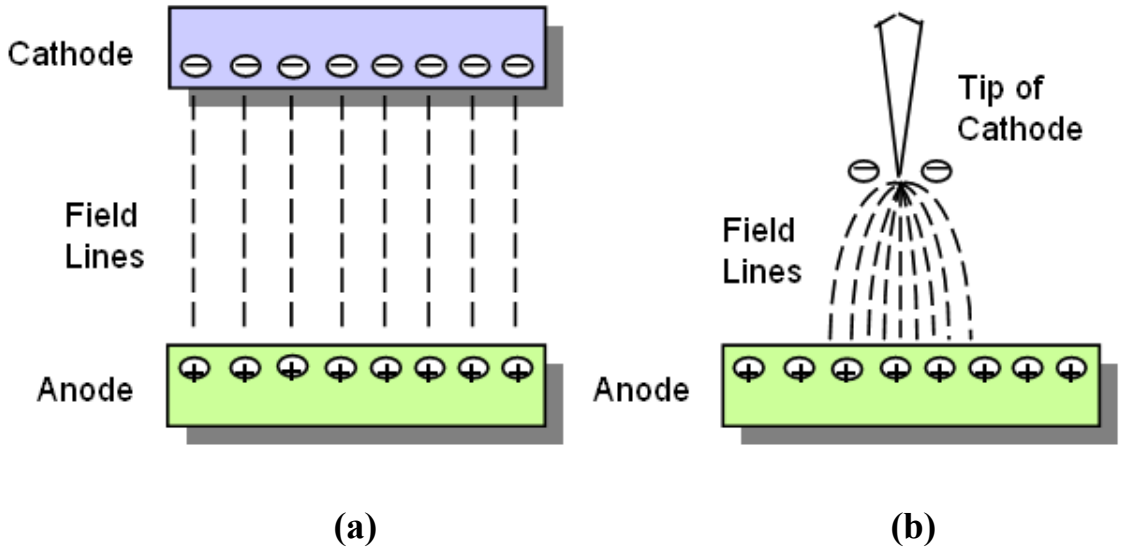

Figure 1-2. Generation of the electric field. (a) When a potential is applied across two plates, (b) When the cathode is a fine tip.

Figure 1-2 shows how a very high electric field can be generated at the tip of a fine point on a cathode. When a potential is applied across two plates, the charges are spread along the plates and a disperse electric field rises. On the other hand, when the cathode is a fine tip, the field lines from the anode concentrate at the tip, resulting in the formation of a very strong electric field at the tip of the cathode like (b).

1.2 Thesis Outline

The central focus of this thesis is silicon patterning of nanostructures that is desired for many electronic, MEMS, photonic, and energy applications and we emphasize two areas of Si nanopatterning below.

In Chapter 2, we can provide benefits by employing magnetically guided chemical etching. According to this technology, one or more ferromagnetic metal catalyst in parallel line array is placed on Si, and the applied magnetic field accurately guides the direction of the vertical slicing without undesirable, off-axis slicing. The magnetostatic attractive force also accelerates the descending speed of the catalyst lines for more rapid slicing speed.

In chapter 3, we have developed ultra-high-density nanopatterns and method of making the same. The method includes localized oxidation of nano-islands on a substrate surface due to applied voltage through the tips of a patterned array of nanoprobes, followed by a pattern transfer by reactive ion etching.

1.3 References

[1] T. R. Albrecht and C. F. Quate, J. Appl. Phys. **62**, 2599 (1987).

[2] C. M. Mate, G. M. McClelland, R. Erlandsson, and S. Chiang, Phys. Rev. Lett. **59**, 1942 (1987).

[3] U. Landman, W. D. Luedtke, N. A. Burnham, and R. J. Colton, Science **248**, 454 (1990).

[4] T. R. Albrecht and C. F. Quate, J. Vac. Sci. Technol. **A6**, 271 (1988).

[5] G. M. Shedd, and P. E. Russell, Nanotechnol. **1**, 67 (1990).

[6] H. J. Mamin and D. Rugar, Appl. Phys. Lett. **61**, 1003 (1992).

[7] E. S. Snow and P. M. Campbell, Appl. Phys. Lett. **64**, 1932 (1994).

[8] C. S. Dulcey, J. H. Georger, D. A. Stenger, T. L. Fare, and J. M. Calvert, Science **552**, 551 (1991).

[9] M. J. Lercel, R. C. Tiberio, P. F. Chapman, H. G. Craighead, C. W. Sheen, A. N. P arikh, and D. L. Allara, J. Vac. Sci. Technol. **B 11**, 2823 (1993).

[10] C. R. K. Marrian, F. K. Perkins, S. L. Brandow, T. S. Koloski, E. A. Dobisz, and J. M. Calvert, Appl. Phys. Lett. **64**, 390 (1994).

[11] W. T. Muller, D. L. Klein, T. Lee, J. Clarke, P. L. McEuen, and P. G. Schultz, Science **268**, 272 (1995).

[12] H. Sugimura and N. Nakagiri, Langmuir **11**, 3623 (1995).

[13] J. C. Kim, Y. Oh, H. Lee, Y. W. Shin, and S. W. Park, Jpn. J. Appl. Phys. **37(12B)** 324 (1998).

CHAPTER 2: Magnetically Guided Nano-Micro Shaping and Slicing of Silicon

This chapter, in full, has been prepared for a manuscript for publication, "Magnetically Guided Nano-Micro Shaping and Slicing of Silicon", Young Oh, Chulmin Choi, Daehoon Hong, Seongdeok Kong, and Sungho Jin. The dissertation author was the primary investigator and author of this paper.

2.1 Introduction

Silicon is one of the most important materials in the semiconductor industry that has attracted much attention for many decades. Generally, silicon geometry needs to be physically processed and shaped by processes including dry etching or wet etching before it can be used in devices or circuits. Physical processing involves cutting, grinding and blade dicing, or patterning for formation of specifically designed lines, grooves, pores or vertical columns. The problem with conventional slicing technique is that silicon could easily be mechanically damaged, the slicing throughput is relatively low, e.g., with saw blade or laser cutting, and that a significant amount of silicon could be naturally discarded during the process, for example, by cutting with a blade having a finite thickness. These problems lower productivity and raise device cost. A dry etching (or reactive ion etching), which can produce a certain pattern or array on silicon, can be performed in parallel fashion using photolithography masking, but this is a rather slow and expensive processing. Wet etching is relatively simpler and cheaper but a well controlled etching and slicing of silicon at a desired speed is often difficult.

Because of the much increased demands for silicon for semiconductor devices and solar cells, the availability and pricing of silicon material have become important practical issues, and it would be highly desirable if silicon can be sliced or patterned in a massively parallel manner for economical processing with minimal waste of material. This invention describes a new magnetically guided semiconductor slicing technique and device applications using such thin sliced semiconductors including silicon, germanium or alloys containing Si, Ge, or both.

Recently a wet chemical, electroless etching method using a metal as a catalyst has been reported for silicon nanowire array or porous silicon fabrication for various potential applications such as photonic [1-3], photovoltaic [4,5], solar cells [6,7], capacitors [8,9], membrane [10], and through-wafer interconnections [11-13]. The kinds of catalyst metal used include gold [14], silver [15,16], and platinum [17] and the chemical etching solutions include H_2O_2 as oxidizing agent and HF to dissolve oxide. When silicon particles were placed on a silicon substrate and they are dipped into an etchant solution including HF and H_2O_2, etching begins from the contact interface between metal particles and silicon substrate. In time, the metal particles penetrate the silicon forming pores, and a sufficient pore formation also results in vertically aligned nanowires of silicon. However, these processes produce irregular nanowires or nanopores rather than the desired slices. The etch speed relatively slow, and the direction of the chemical etching sometimes deviate from the desired vertical direction.

This invention overcomes such problems by employing magnetically guided chemical etching. According to the invention, one or more ferromagnetic metal catalyst in parallel line array is placed on Si, and the applied magnetic field accurately guides the

direction of the vertical slicing without undesirable, off-axis slicing. The magnetostatic attractive force also accelerates the descending speed of the catalyst lines for more rapid slicing speed.

2.2 Materials and Methods

2.2.1 Silicon slicing

Instead of metal particles, we formed metal line patterns with a triple-layer configuration as illustrated in Figure 2-1, with the ferromagnetic catalytic magnetic layer line such as Fe sandwiched by catalytic Au layer lines. The ferromagnetic layer in the middle provides magnetic force for vertical or guided-direction movement of the catalytic lines while the Au layer reacts with the chemical etchant such as an etchant solution including HF and H_2O_2 to induce vertical etching.

This method enables a kind of plane etching without forming silicon nanowire because it can maximize physical contact with the silicon substrate during initial etching and etch two times at the same position by double Au layers.

We used a p-type Si (100) wafer (boron-doped, 10-20 Ω ㎝) with thickness of 550 ㎛ and one side was mirror-polished. Before the experiment, this silicon wafer is thoroughly cleaned according to the standard RCA procedure [18,19]. Figure 2-1 shows the simple schematic for this experiment. The wafer was cut into 20 × 20 ㎟ area to conveniently conduct the experiment.

As illustrated in Fig. 2-1, the sample surface was first pre-patterned with a grooved line array {Fig. 2-1(a)} by photolithography or nanoimprinting lithography (NIL) with SU-8 photoresist, ~2 ㎛ thick or PMMA resist, ~ 300nm. The polymer resist lines were 10 ㎛ wide x 20 ㎛ spacing apart. A narrower pattern of 5 ㎛ wide x 10 ㎛ spacing has also been demonstrated. Next, many parallel micro-lines of a stacked Au-Fe-Au triple layer (with a thickness of 10 nm, 10 nm, and 10 nm, respectively) were deposited on the resist-patterned silicon groove using sputtering or thermal evaporation {Fig. 2-1(b)}. The sample so prepared was then placed in a teflon beaker etching bath containing a mixture solution of diluted hydrofluoric acid and hydrogen peroxide (with a volumetric ratio of HF: H_2O_2: H_2O = 5: 45: 15) at room temperature. While the sample is in the solution, a permanent magnet (NdFeB) placed in the bottom area of a teflon beaker {Fig. 2-1(c)} supplies directionally (vertically) attractive force pulling the ferromagnetic Fe lines sandwiched between two Au catalyst lines. At a given time of etching of ~12-16 hours, the silicon wafer (e.g., 250 - 550 ㎛ thick wafer) can be sliced completely {Fig. 2-1(d)}. And the acetone and gold etchant are used to remove the remaining PMMA resists and the remnant three layer metals. The completely sliced silicon is washed thoroughly using deionized water.

According to this technology, a multilayered (Au/Fe/Au)n (where n=1 – 20) can be utilized for more powerful magnetic guiding, for further accelerated etching/slicing speed due to the increased magnetic material. The multilayer configuration also makes the Si etching/slicing continue for longer time and thickness.

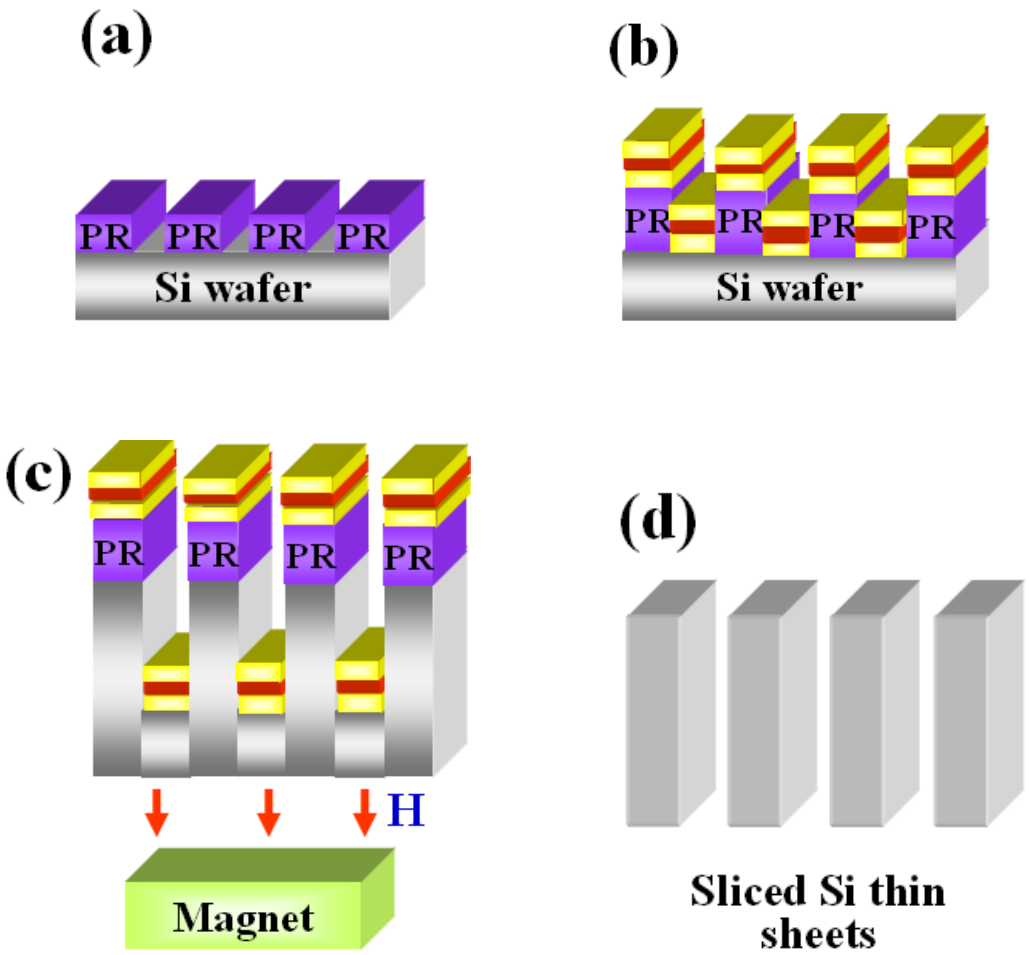

Figure 2-1. Magnetically direction-guided silicon slicing process. (a) Photoresist (PR) line pattern on Si surface, (b) (10 nm Au/ 10 nm Fe/ 10 nm Au) thin film catalytic trilayer deposition by sputtering, (c) Field-accelerated, guided electroless etching/slicing into Si, (d) Resist lift-off and Au catalyst film removal to obtain thin Si sheets.

2.2.2 Magnetic particle coated with Au

200 mL of aqueous solution containing 250 μL of aqueous 10 % (w/v) $HAuCl_4$ was boiled and then 3.5 mL of 1 % sodium citrate tribasic dihydrate was added. After the color of the solution changed from black to wine red, the solution cooled down to room temperature and the gold nanoparticles were washed with fresh D.I. water. The prepared gold nanoparticles were added to 2 mL of thiol-attached magnetic silica bead (10 mg/mL) with vigorous stirring and then the reaction kept for 24 h. 2.22 g of NH_2OH and 500 μL of aqueous 10 % $HAuCl_4$ were mixed with gold-monolayer magnetic silica bead with vigorous stirring. After 24 h, the particles were washed with fresh D.I. water.

2.2.3 Silicon nanowires fabrication

The composition ratio of the solution is 4.6M HF to 0.02M $AgNO_3$ (v/v = 1/1) [20, 21]. After submerging the sample for about 20 minutes in this solution and washing silver dendrites attached to the silicon surface in HNO_3/H_2O solution, it is cleaned with deionized water. All the experiments described here were performed at 50 °C.

2.2.4 Characterization

The cross-sectional and top-surface images of the sliced silicon were was analyzed by a field emission scanning electron microscope (XL30 ESEM, Philiips). Optical intensity measurements were performed with a ZEISS AXIO observer spectrophotometer.

2.3 Results and Discussion

2.3.1 Silicon etching by magnetically guided field

2.3.1.1 Silicon slicing applications

Based on prior studies, etching of Si using particles such as Au, Pt or Ag has been reported [16,17]. In Equation 1, etching began by reducing H_2O_2. Generally, the silicon etching process is slow due to the low catalytic capability of silicon in an HF- H_2O_2 solution.

$$H_2O_2 + 2H^+ = 2\,H_2O + 2h^+ \qquad (1)$$

The metals mentioned above are used as a catalyst to produce positive holes in silicon as it donates electrons to H_2O_2 and takes in electrons from the silicon. As shown in Equation 2, the positive holes produced make oxidative dissolution of silicon in solutions that include HF. Since this mechanism occurs on the interface contacting with metals, etching process is conducted continuously in the surface in contact with metal.

$$Si + 4h^+ + 6HF = SiF_6^{2-} + 6H^+ \qquad (2)$$

Figure 2-2 shows the Au film that has been deposited on the silicon through thermal evaporation process in order to determine the optimal thickness of the Au film when slicing the silicon. To check on the degree of chemical etching, Au film was deposited on the left side only, without any deposition on the right side. If the Au film is

3nm or 5nm thick, small domains exist separately from each other on the surface of the Au film, as shown in Fig. 2-2(a) and 2-2(b). We can see that after about an hour of guided chemical etching, no more etching was occurring where there is no Au film and there remain numerous undesirable silicon wires on the surface where there was no contact with Au domains. In other words, it can be said that no silicon etching was accomplished where there is no Au domain. We can see that under the same condition, a 5nm thick Au formed the more compact wire than a 3nm thick Au from the lower's small right images. However, this experimental condition was inappropriate to perfectly slice the silicon. In the case of a 10nm thick Au, Au domains are arranged relatively compact and, therefore, the remaining silicon wires are relatively small and short while a kind of plane etching is done relatively well, as shown in Fig. 2-2(c). With 13nm thickness, Au domains exist in continuous condition in many areas as we observe the surface before etching from Fig. 2-2(d). Plane etching was done the small area where Au film exists like the case of 10 nm during etching because many parts of the Au film peeled off easily from the silicon due to the continuous Au films. Therefore, there is a critical thickness of Au layer to enable clean Si slicing, which was determined to be ~10 nm in this series of magnetically guided slicing experiments.

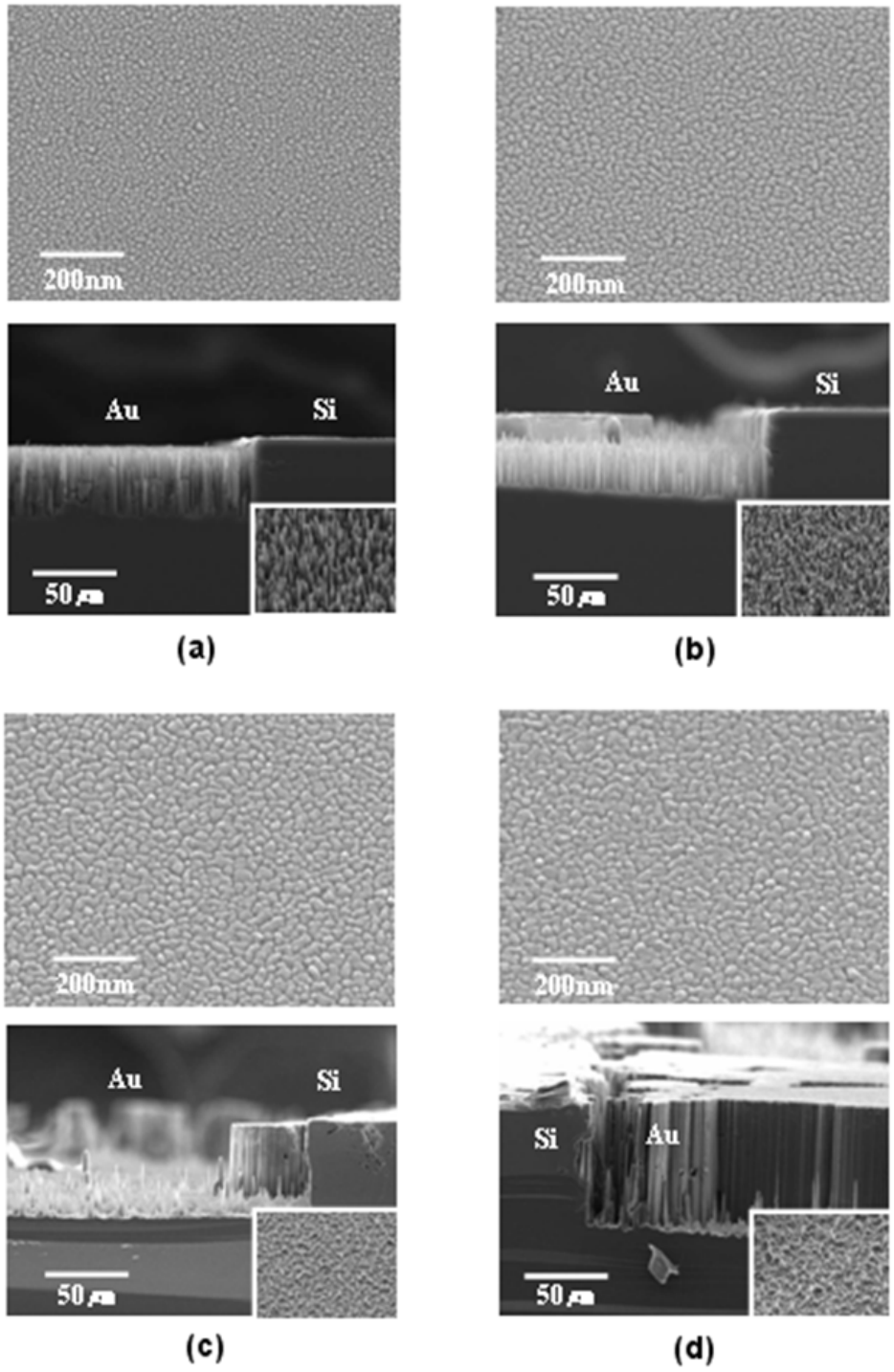

Figure 2-2. The upper row of SEM pictures show morphology after Au is deposited on he silicon substrate and the lower images are cross-sectional views and top views of the etched surface after etching for one hour. (a) 3nm, (b) 5nm, (c) 10nm, (d) 13nm

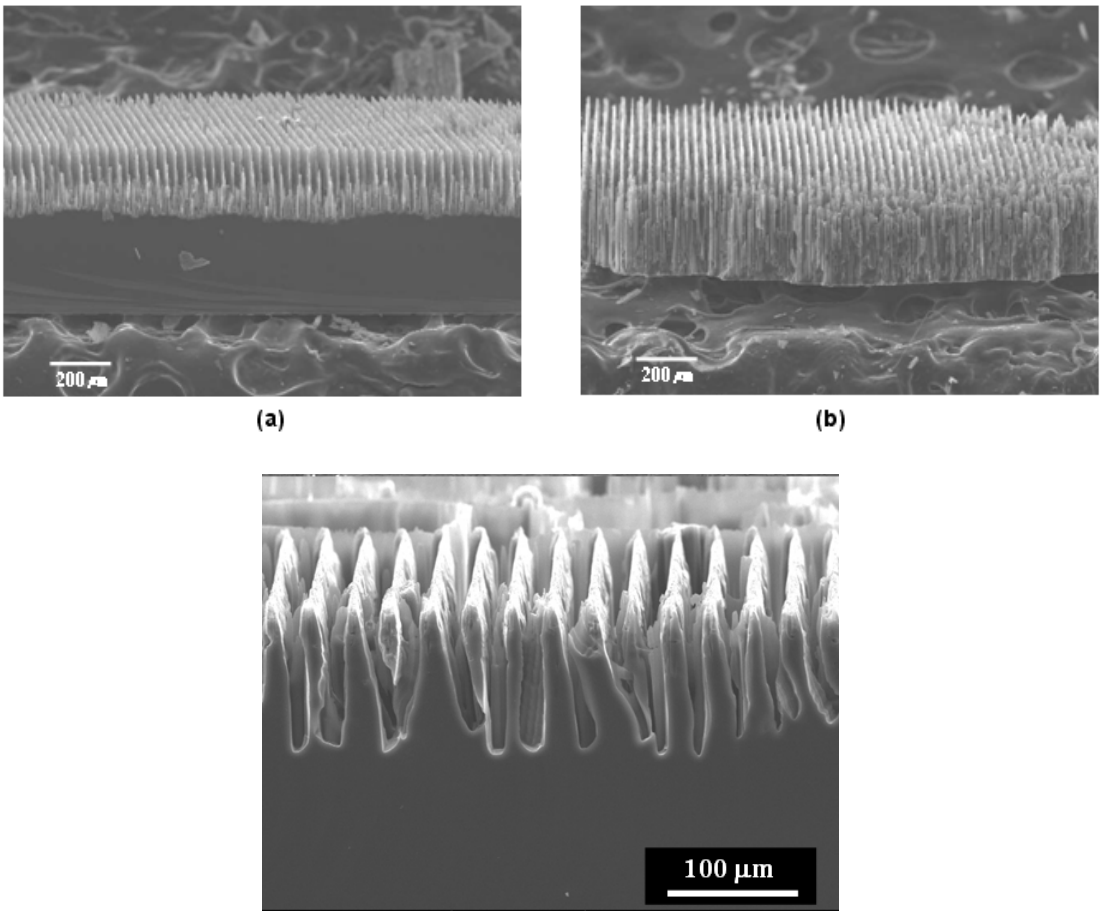

Figure 2-3. SEM images showing sliced silicon wafer conducted using parallel line patterns. Au 10nm film : (a) 4h etching, (b) 12h etching. Au/Fe/Au = 10/10/10nm film : (c) Silicon slicing by magnetic tri-layers but without applied magnetic field (2 hrs slicing).

Figure 2-3(a) and (b) show that silicon was etched after the line pattern was created on the silicon through the NIL method and deposited 10 nm of Au, which is the optimal condition for plane etching. Initially, silicon is sliced following the shape of the pattern transferred earlier. However as the chemical etching continues, we observe a formation of numerous undesirable silicon wires produced almost continuously on the whole area, rather than the Si wafer being sliced in a neat manner according to the Au catalyst line pattern deposited. Consequently we fail to completely slice silicon substrate. In case of figure 2-3(c), if the magnetic trilayer is used but no magnetic field is applied, the vertical etching still tends to be irregular with wire-like or crooked shaped geometry. An improved slicing technique was therefore necessary. With the presence of magnetic attraction below the silicon, the Fe film in the middle can prevent Au films from peeling off easily on the silicon substrate, which could happen in initial etching, and the occurrence of silicon nanowires can be reduced by inducing consistent physical contact with the Au films and the silicon. More importantly the magnetic layer such as Fe, Co, Ni, and their alloys enables magnetically direction-guided chemical etching, along the exact vertical direction for the straightforward slicing purpose, or at an angle for other device applications requiring tilted slicing or groove formation for devices requiring different Si crystal orientations. The applied magnetic field accurately guides the direction of the vertical slicing without undesirable, off-axis slicing. The magnetostatic attractive force on the ferromagnetic layer also accelerates the descending speed of the catalyst lines for more rapid slicing speed.

In addition to the advantages of the magnetically guided Si etching discussed above, i.e., enabling the slicing into micro sheet geometry, and direction-controlled

slicing to any crystallographic orientation, there is also another important kinetic advantage when the magnetic etching is utilized. The application of magnetic field accelerates the rate of Si etching as shown in Fig. 2-4, presumably do to the magnetic attractive force pulling down the etch lines downwards. The stronger the applied field is, the faster the Si slicing kinetics become. The presence of magnetic field during the Si slicing using Au/Fe/Au trilayer line arrays accelerates the etching speed, e.g., by ~300% when the applied field is increased from ~300 Oe to ~1,500 Oe (see Figure 2-4). This is attributed to the enhanced magnetic pulling force under stronger applied magnetic field. The magnetic field strength in this case was controlled by simply adjusting the gap distance between the magnet face outside the Teflon beaker and the Si work piece immersed within the etchant in the beaker. The magnetic field was measured by using a typical gaussmeter.

The morphology and dimension of the magnetically guided, vertically sliced Si microsheets are described in Fig. 2-5(a)-(c) with some example SEM images. Figure 2-5(a) and (b) demonstrate a parallel and simultaneous slicing of many ~10 μm thick Si slices. The loss of Si material by slicing is very small in our processing method (as compared to the typical 150 – 200 μm kerf loss in wire saw cutting). In the example case of Fig. 2-5(c), the loss was ~15μm width per cut.The quality of sliced Si surface was relatively smooth. For enhancement of sunlight absorption, a roughened surface is actually desirable anyway. A further intentionally roughened surface of active photovoltaic Si surface, e.g., with induced surface Si nanowire forest as will be discussed later, may optionally be used to reduce sunlight reflection for capturing and utilizing as much sunlight energy as possible.

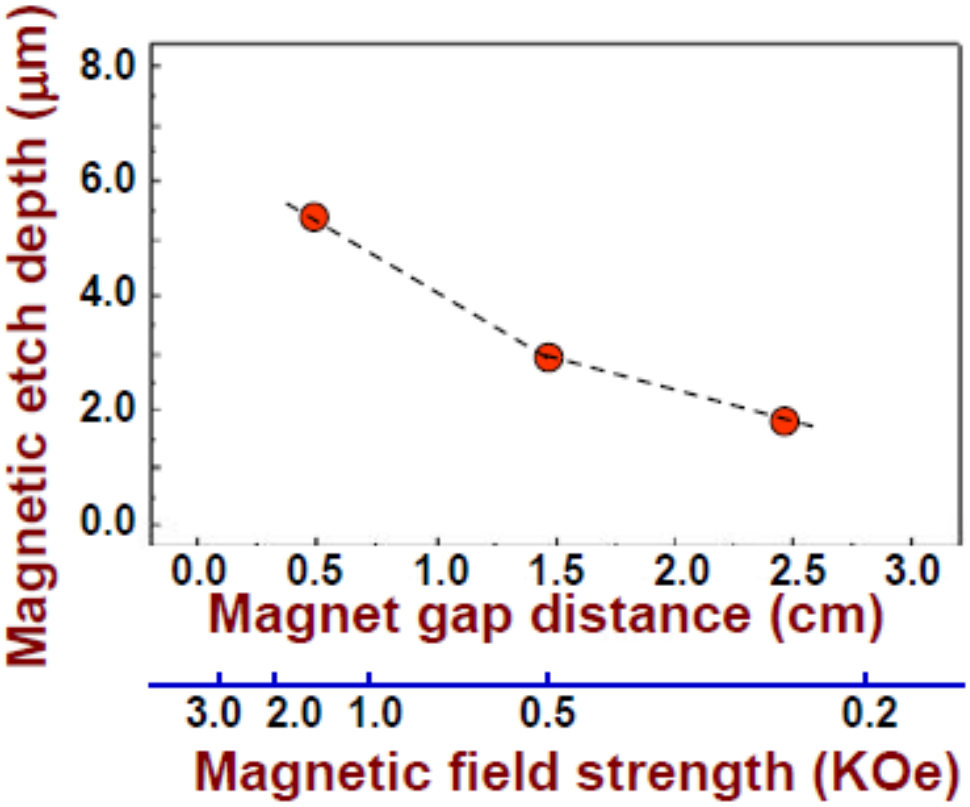

Figure 2-4. The effect of applied magnetic field strength on the kinetics of magnetically guided Si slicing. The Nd-Fe-B permanent magnet was positioned at different distances to change the applied magnetic field strength.

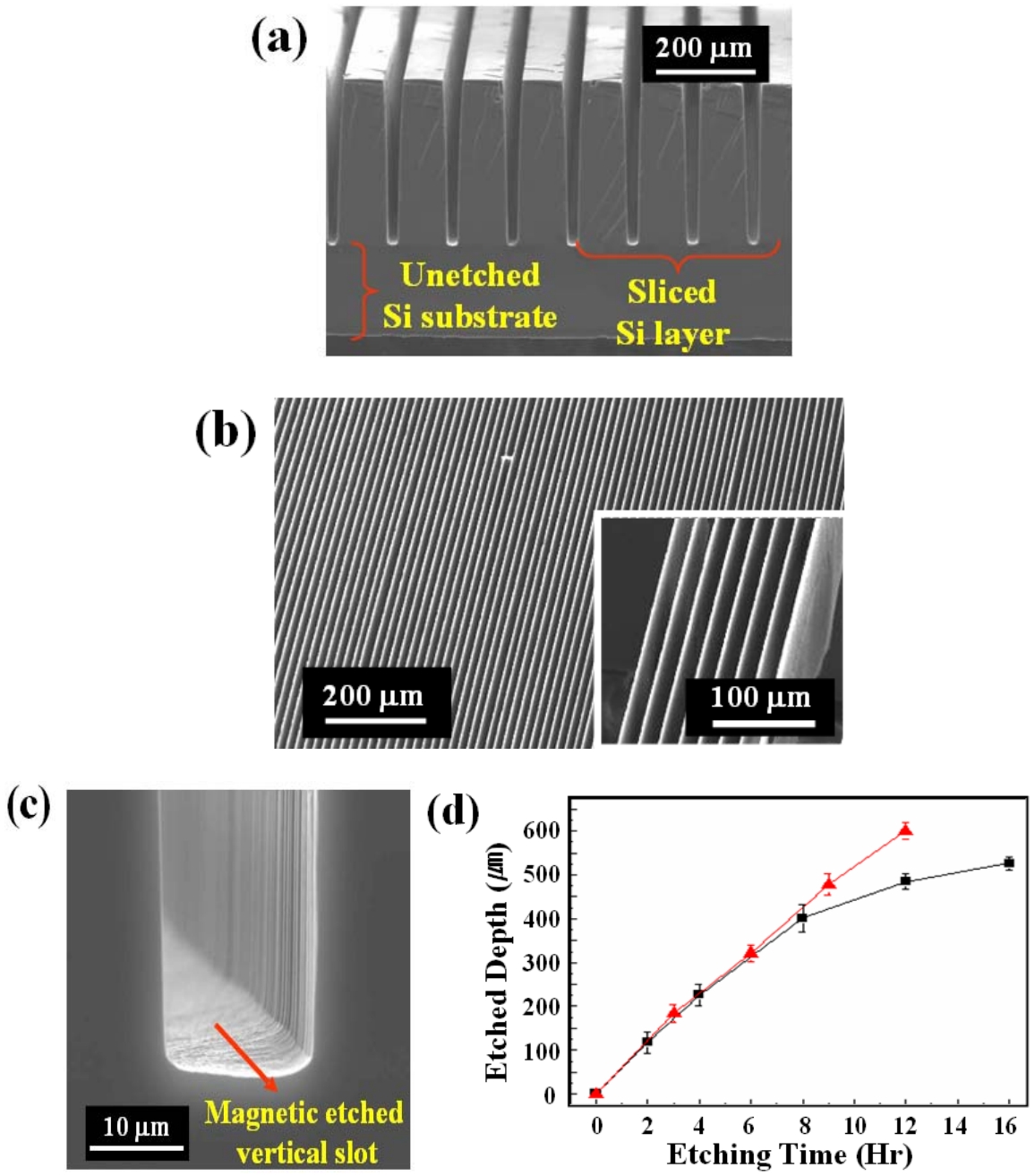

Figure 2-5. SEM pictures of vertically magnetically guided Si slicing to ~10 µm thickness. (a) A partially sliced array of thin Si sheets after 2 hrs etching, (b) complete slicing after 12 hrs (the inset = higher mag image), (c) a magnified image of the etched slot, (d) a plot of the etched depth of vs etch time. (red : etching solution changed every 6hr, black : no solution change).

The slicing depth is dependent on the etching time, the concentration of the electroless etching solution as illustrated in Fig. 2-5(d). A periodic replenishing of etching solution or active stirring substantially increases the slicing speed. The slicing speed is also dependent on the magnitude of the applied magnetic field since the magnetic attractive force exerts a vertical pull-down force on the Au/Fe/Au triple layer that causes the catalytic Si etching. It was experimentally observed that an increase of average applied magnetic field from 300 Oe to 3,000 Oe increased the etch rate (slicing speed) by nearly 300%.

For transformative industrial applications of thin Si, a high-speed etching/slicing is an important parameter as it relates to manufacturing throughput and ultimate materials/devices cost. Indeed, simple changes in the processing conditions such as an increase of HF concentration and bath temperature resulted in a striking ten fold increase in the Si slicing rate to ~500 μm/hr as shown in Figure 2-6. Additional optimization of process parameters is likely to further increase the etch rate. An ability to slice thick Si ingot is also an important aspect. Au serves as a catalyst, so it is not consumed during the etching/slicing process, as we were able to carry out magnetically guided, vertical Si etching for at least up to 0.8 cm depth (using thick 0.8 -1.0 cm thick Si pieces) with the same, thin Au/Fe/Au etch line (data not shown).

The etch rate increased from ~50 μm/hr for HF solution (1.87 M, corresponding to ~7.7wt % HF) at room temperature (18^{o}C) to ~120 μm/hr for HF solution (3.73 M) at the same room temperature, to ~500 μm/hr for HF solution (3.73 M) at an elevated bath temperature of 50^{o}C. The Si slicing is conducted in a massively parallel way. For the case of 5 μm thick Si slicing with 5 μm spacing, assuming a starting Si ingot of 20 x 20 cm^2

area in each bath, there would be 20,000 lines simultaneously being etched, with the slicing time per cut (through an assumed Si ingot thickness of 1cm starting material) estimated to be ~10^4 μm thickness divided by [(500μm/hr) x 20,000 slices] = ~3.6 seconds/slicing, a rather fast slicing rate. Since a larger-area or longer-ingot Si can be used as a starting material, or hundreds of multiple baths could be operated simultaneously without sophisticated or costly sawing equipment involved, the average time and cost for Si slicing could be further reduced.

The magnetically sliced Si is essentially stress-free, as compared to the case of traditional mechanical saw-cut Si wafers that produces strained, chipped and rather rough Si surface. This is due to the chemical etching based slicing. The surface quality of the magnetically sliced Si is surprisingly smooth, in contrast to the rough/granular surface of the wire-saw cut Si. The average surface roughness measured by AFM was R_a ~7 nm and the root-mean-square roughness R_{rms} ~13 nm as shown in Figure 2-7. However, as the etching rate is rapidly increased, the surface roughness of sliced silicon is increased as shown in Figure 2-8. The average surface roughness measured by AFM was R_a ~11 nm and the root-mean-square roughness R_{rms} ~18 nm

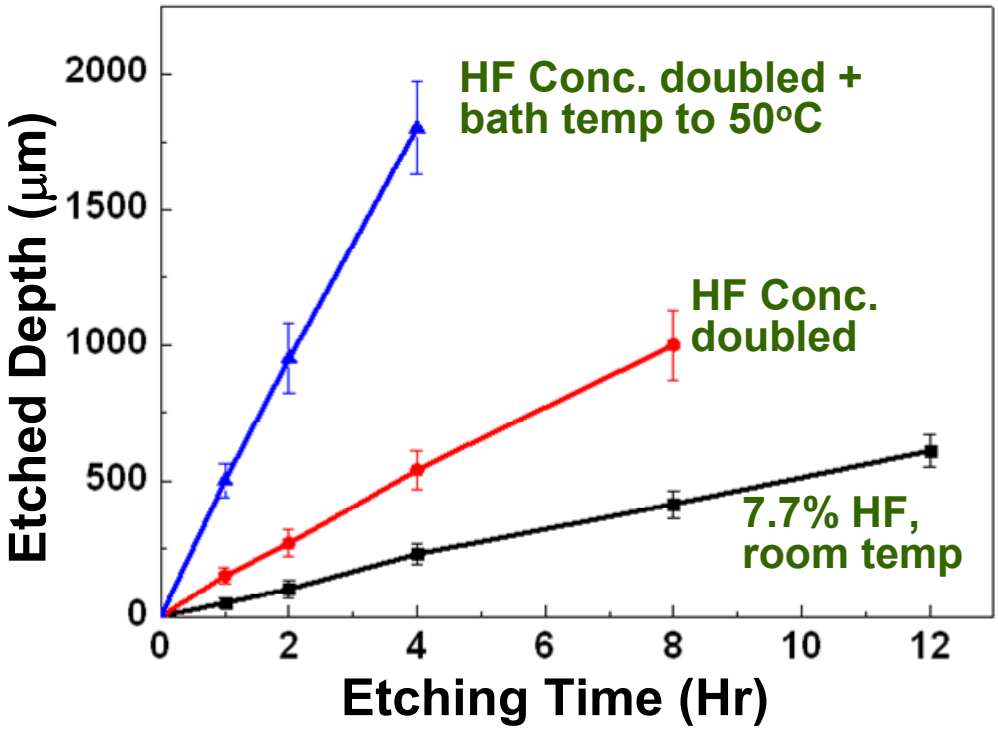

Figure 2-6. Magnetically guided Si slicing etch rate altered by acid concentration and bath temperature employed.

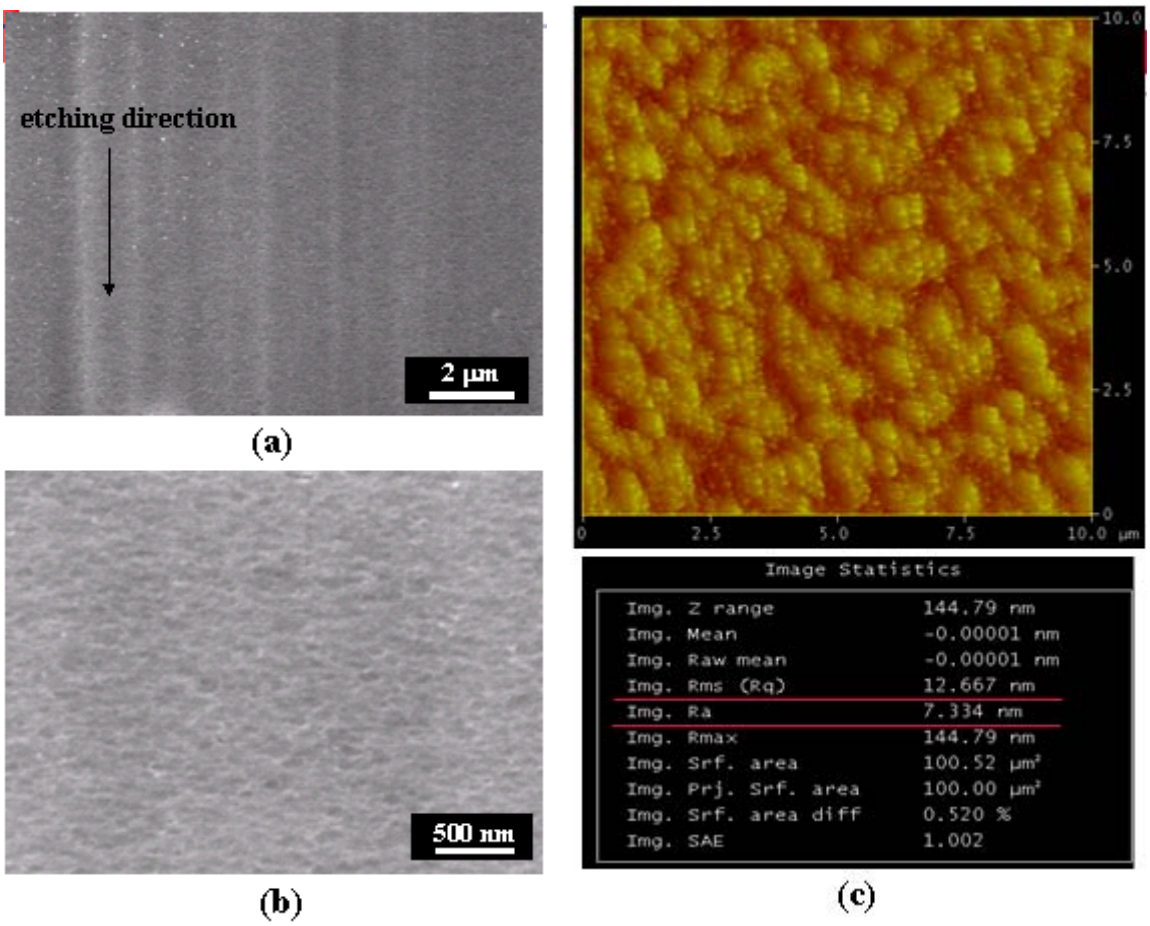

Figure 2-7. SEM micrograph showing the surface roughness of the 10 µm thick Si microsheet slices produced by magnetically guided Si etching (Fig. 2-6 black color conditions, 3 hr), using 10nm Au / 10nm Fe / 10 nm Au trilayer catalytic etch line array. (a) low magnification SEM micrograph taken at 45^{o} oblique angle, (b) higher magnification SEM showing a relatively smooth surface, (c) AFM image and surface analysis

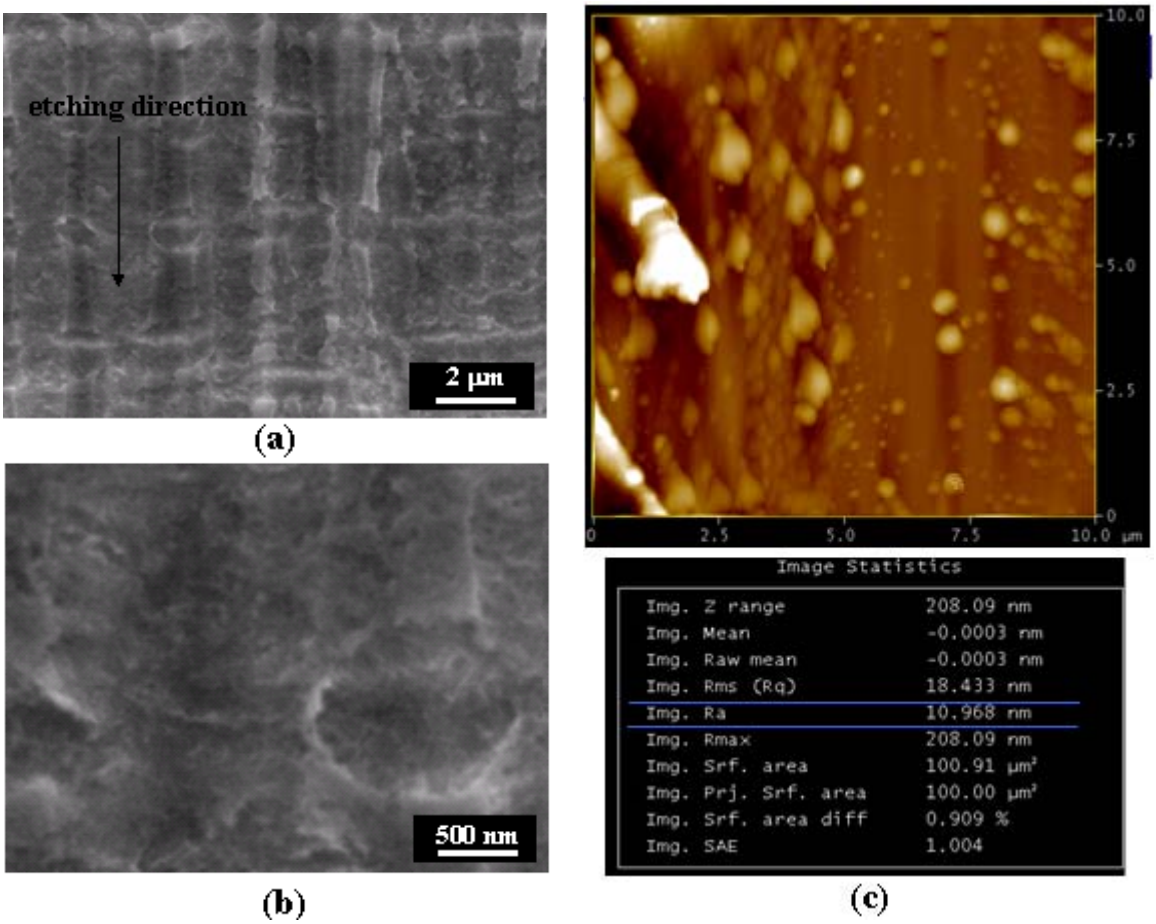

Figure 2-8. SEM micrograph showing the surface roughness of the 10 μm thick Si microsheet slices produced by magnetically guided Si etching (Fig. 2-6 blue color conditions, 1 hr) using 10nm Au / 10nm Fe / 10 nm Au trilayer catalytic etch line array. (a) low magnification SEM micrograph taken at 45^{o} oblique angle, (b) higher magnification SEM showing a relatively rough surface, (c) AFM image and surface analysis

2.3.1.2 Solar cell applications

Single crystal Si ingots or boules are typically prepared by crystals growth techniques such as the Czochralski process which utilizes crystal seeds for growth of large diameter Si ingots, for example, 8 inch diameter and many feet long ingots. For wafer slicing, the novel magnetically guided etching technique can be used as more efficient, material saving method for producing thin wafers than the typical wire saw slicing technique. One of the convenient techniques for slicing of such round ingots using the this technology method is to utilize a curved shadow mask that conforms to the round geometry of the ingots, either elastically or pre-bent to fit the ingot boule curvature. Such a shadow mask can be made of, for example, with a curved metal foil containing parallel line shaped slots through which the magnetic metal/noble metal multilayers can be deposited on the ingot surface as a zebra shape pattern for subsequent etching/slicing. Such a shadow mask can also be used to selectively photolithographically pattern a coated resist such as PMMA layer on the ingot surface, e.g., by UV exposure of stripe pattern on the ingot surface already containing surface magnetic metal/noble metal multilayers. An example shadow mask geometry is a zebra pattern on curvatured stainless steel mask having a radius of curvature of 4 inches, with 50,000 slots of 5 micrometer width and 10 micrometer spacing (to produce 10 micrometer thick wafer slices by the guided etching) , or 10 micrometer width and 100 micrometer spacing (to produce 10 micrometer thick wafer slices).

An alternative approach is to use a microstamp having a conforming geometry for the curved ingot surface in such a way that a pattern of resist lines (or an absence of resist lines) can be stamped on the ingot surface, with the magnetic metal/noble metal

multilayers either pre-deposited or deposited after the resist patterning for lift-off process.

For efficient solar cell applications, it is highly desirable to have large surface area, as well as sufficient light absorption with minimal sunlight reflectance. Vertical Si microlayer array (5-10 μm thick Si layer slicing by magnetic etching) was subjected to additional surface structure modifications with sideway Si nanowire formation by employing additional catalytic etching using $AgNO_3$ solution (electroless etching) as shown in Fig. 2-9. While the surface nanowires (~3-20 nm diameters) in Fig. 2-9 may not be the most optimal configuration for solar cells, it is demonstrated that such surface nanowires enhance light absorption on these vertical Si micro-layer array of Fig. 2-11. The light absorption data is shown in Fig. 2-11. As one of the optional designs of solar cell construction, the surface of the micro Si layers can be coated with either Si nanowires or microwires in combination with by n-type doping (e.g., by plasma enhanced chemical vapor deposition (PECVD) to form large-surface-area p-n junctions.

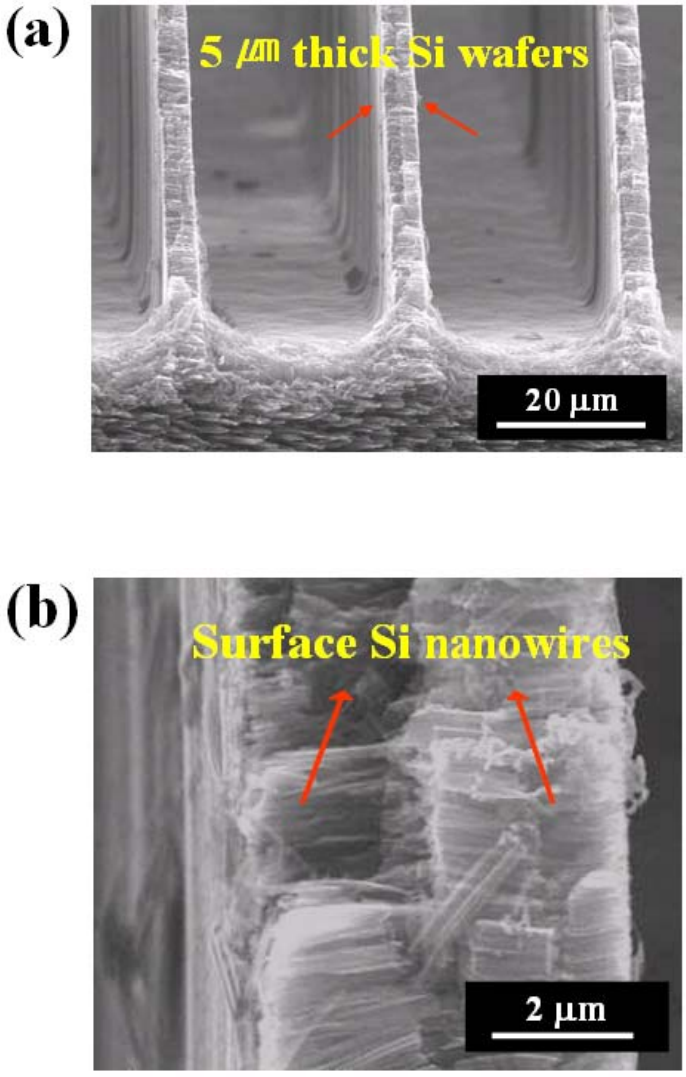

Figure 2-9. Thin 5 μm thickness Si layer slicing by magnetic etching, using Au/Fe/Au catalyst line array (as shown in Fig. 2-1), followed by electroless etching using $AgNO_3$ solution to demonstrate the formation of sideway branching of Si nanowires (shown in the inset by a higher mag. SEM image). No magnetic field was used for the branching etch process.

Shown in Fig. 2-10(a) is an SEM micrograph for thin 20 μm wide, sliced Si layer array (not through-cut) for possible vertical solar cell array structure. The slicing was halted before through cut all the way so as to retain some of the bottom base Si material to serve as a support for the vertically positioned, parallel Si slices. The bottom surface of the Si base is desirably metal-coated, e.g., with Al, for light blocking and electrical conduction (not shown). On the surface of each of these 20 μm thick layer on both sides, either Si nanowire by catalytic etching (e.g., ~20 nm diameter and 2 μm tall as depicted in Fig. 2-9) for enhanced light absorption, or nanopillars (0.3 – 1 μm dia and 8 μm tall) are formed by sidewall Si etching using deposited mask islands for increased p-n junction area, or a combination of both. We have demonstrated a principle of such branch Si pillar formation for hierarchical Si structures using anodized aluminum oxide (AAO) template method or Ag thin film 400 ℃ ball-up approach to form metal island masks, followed by high pressure RIE etching (not shown).

The resultant vertical nano solar cell array, Fig. 2-10(b), could be one of the possible architectures for three-dimensional solar cells with potentially substantially improved solar cell efficiency due to the increased active p-n junction interface area as well as due to enhanced sunlight absorption aided by Si microwalls and nanowire structures. The enhanced light absorption by the surface nanowire addition is indirectly indicated by reduced sunlight reflectivity as shown by experimental data in Fig. 2-11.

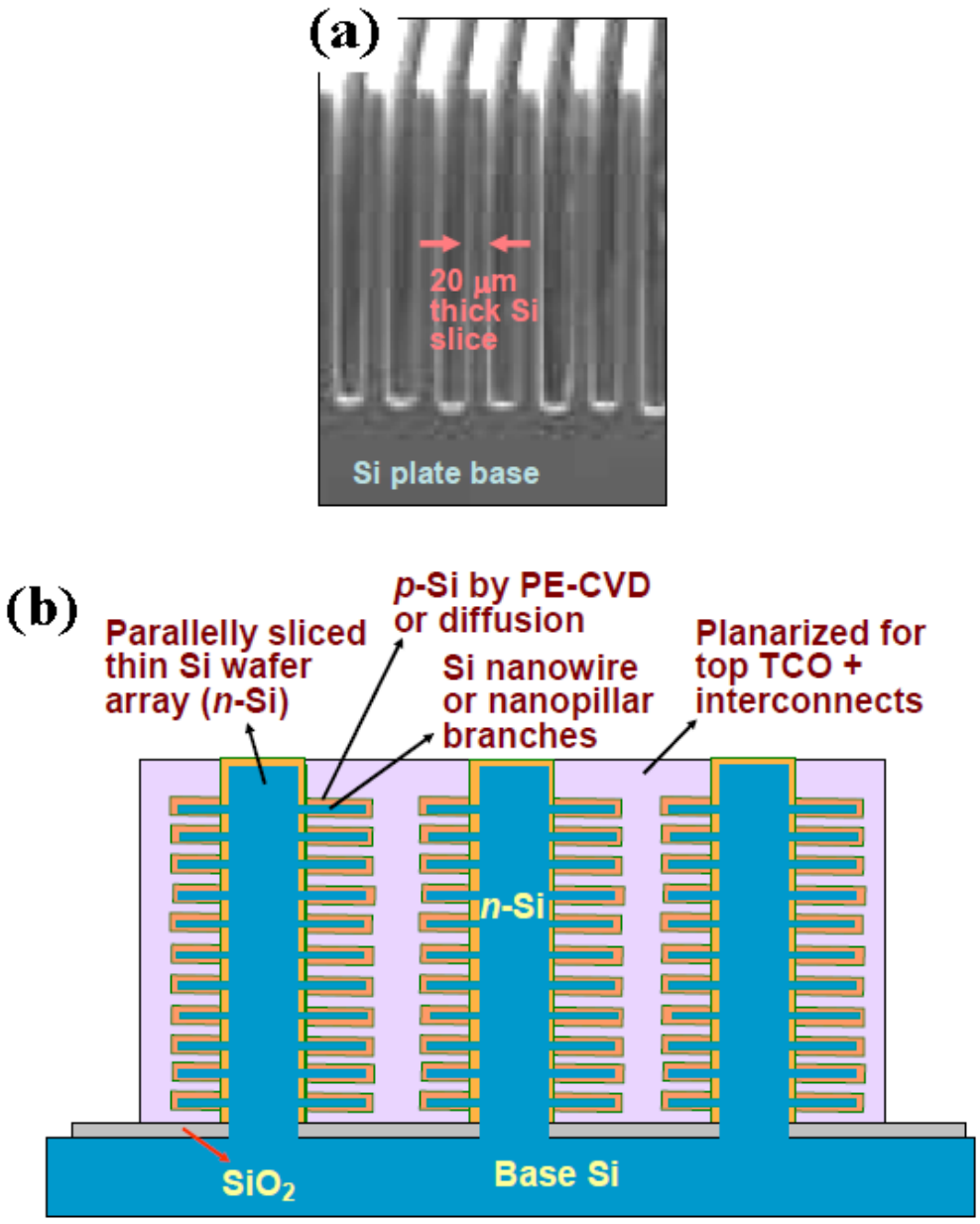

Figure 2-10. (a) Thin 20 μm wide, parallelly sliced Si layer array (not through-cut) for vertical solar cell array structure. (b) Horizontal surface Si nanowires or nanopillar arrays are added for increased p-n junction surface area or enhanced light absorption.

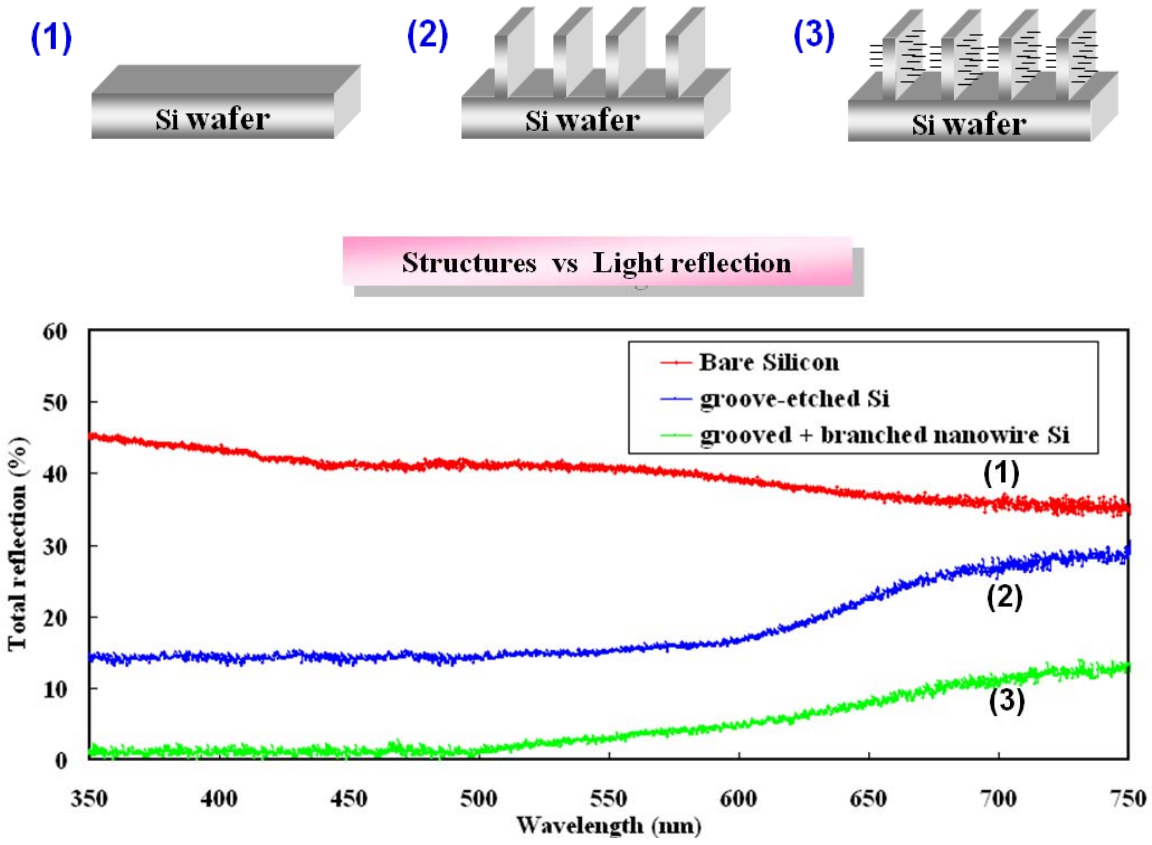

Figure 2-11. Comparative light reflectivity measurements on (1) flat Si, (2) parallel wall sliced, vertical Si layer array, (3) sliced Si walls with additionally etched side branches of Si nanowires (~10 nm dia, ~1 μm tall).

For sliced Si sheets, especially the thinner wafers of 10 – 40 μm thickness, careful handling of fragile wafer sheets is necessary. As the Si sheets need to be laterally connected in series or parallel, e.g., using Cu conduction lines for solar panels, the sliced wafers can be placed on a re-usable tray (e.g., having a periodic array of vacuum suction pillars) for safe handling and for automated mechanical and electrical connection assembly into solar panel configurations.

An alternative approach is to avoid such handling of thin wafers altogether, by utilizing intentional incomplete slicing (i.e., leaving some base Si material and not slicing all the way through), as shown in Fig. 2-9, which depicts an example configuration of such a Si vertical array PV solar cell configuration. Micrometer dimension Si vertical arrays could be utilized for viable PV solar cells if properly configured, e.g., with enhanced sunlight collection (more light absorption). The surface of the p-type (or n-type) Si vertical sheets (e.g., 20 μm thick) of Fig. 2-9 and Fig. 2-10 will be coated with n-type Si using PE-CVD deposition to form the p-n junction. Optionally, if side branch Si pillars are added, e.g., via mask island formation and RIE etch (e.g., like Fig. 2-11), the total p-n junction surface area will be much increased. The Fig. 2-12 type array solar cells or its variations provide a 3-D environment which could produce substantially higher solar cell efficiency per unit horizontal area than flat Si solar cells due to the much larger active p-n junction area.

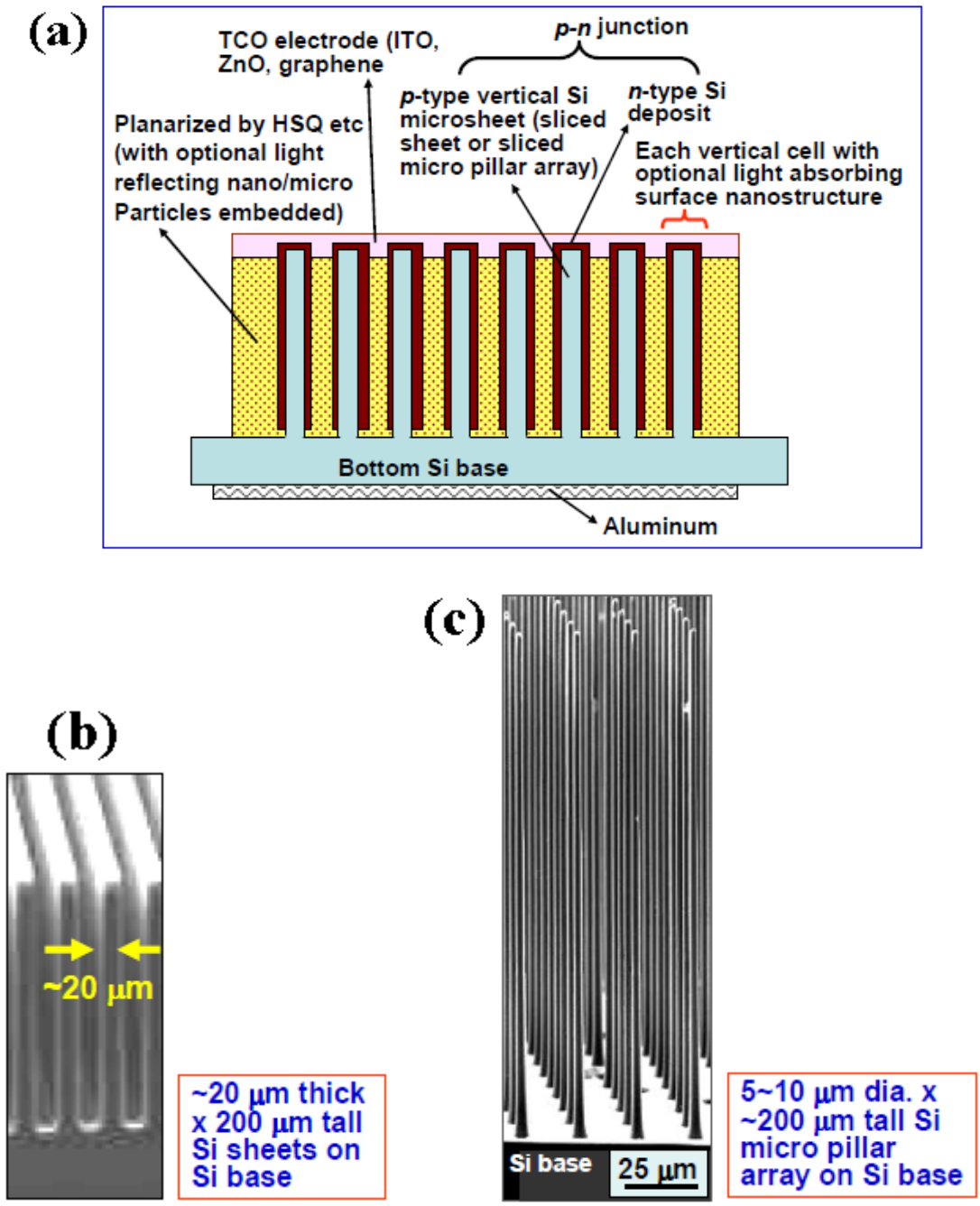

Figure 2-12. (a) Simplified schematic illustrating a possible three-dimensional array of photovoltaic solar cells using non-through-cut Si sliced array of (b) microsheets or (c) micro pillars produced by magnetic guided etching. The array can be planarized so as to enable the positioning of optically transparent upper electrode layer, using a transparent oxide filler space between neighboring solar cell devices. Optional light reflecting nano or microspheres may be utilized for enhanced light collection. Detailed structures are not shown in the figure, such as the dielectric layers, antireflection layers, etc.

Because of the 3-D nature of the non-through-cut Si slice vertical array of Fig. 2-12, it would be difficult to place the upper TCO (transparent conducting oxide) electrode such as ITO layer. According to this technology, a planarization process is employed inserting SiO_2 filler material to the empty space between the vertical Si layers so as to allow the blanket deposition of the transparent conducting layer such as transparent conducting oxide (TCO) like the well known indium tin oxide (ITO), graphene or carbon nanotube network. According to the this technology, a convenient planarization technique is employed by spin coating or dip coating hydrogen silsesquioxane (HSQ) resist liquid (or Si-containing sol-gel precursor liquid) to fill the valley regions, curing and reactive ion etch (RIE) to remove the overfilled excess thickness regions to the desired planarized height so as to expose the top of the Si solar cell electrodes, baking at 110 °C to convert to SiO_2, followed by mechanical hardening by oxygen plasma RF irradiation. The HSQ (and the eventual SiO_2 filler material) could optionally contain light reflecting nano or microspheres such as aluminum oxide or Ag micro particles for enhanced light collection.

With respect to Si shaping into different geometries for other technical applications, an array of tall Si micro pillars can also be easily created using the proposed magnetic guided etching by using a swiss-cheeze configured trilayer of (Au/Fe/Au) instead of line arrays of Fig. 2-5. The swiss-cheeze keeps coming downward while continuously etching the Si, following the magnetic attractive force direction, thus creating a tall and periodic Si micro- or nanowire array. Such a Si micro pillar array with ~2-10 micrometer diameter and very tall (200 – 500 μm) height is also included in Fig. 2-12. Such an extremely high-aspect-ratio Si pillar arrays are typically very difficult to obtain using conventional, prior art photolithography. The magnetically direction-guided

catalytic etching mechanism to create such a tall Si pillar array seems to be similar to that for the parallel line slicing discussed above.

2.3.2 Nonconventional silicon geometry shaping by magnetically guided field

The magnetically guided Si slicing technique can also be useful for creating some nonconventional Si geometry, which can lead to broader scientific research, new device phenomena, and new technological applications.

2.3.2.1 Flexible silicon device

Since our slicing technique can easily produce very thin Si wafers as thin as ~5 μm (and possibly even much thinner), flexible or conformable Si devices and circuits can be constructed from such thin Si wafers. As suggested by recent research, there are many exciting potential applications using thin Si, for example, for flexible displays, sensors, actuators, integration of compliant semiconductor chips for in vivo biomedical applications on curvatured surface. Since the magnetic field guides the direction of Si slicing in the proposed research, there is an intriguing possibility that off-axis orientation Si wafers (e.g., non-(100), (110), (111)), could be created easily. Such different crystallographic orientation of Si wafers enables interesting and new semiconducting, photonic, optoelectronic, and mechanical properties which can be exploited to create new devices with exciting characteristics.

2.3.2.2 Micro curved tunnel formation within silicon crystal

The magnetic slicing technique offers a promise of Si slicing at any desired directions by altering the magnetic field direction, ignoring the crystallographic orientations, as demonstrated in Fig. 2-13 (using 800 Oe magnetic fields). Being able to slice and prepare Si wafers cut along any crystal orientations is likely to open up new perspectives/applications in Si electronics and various other potential applications. Different Si orientations and non-(100) orientations provide different electronic and other physical characteristics, which can be useful for a variety of technical applications.

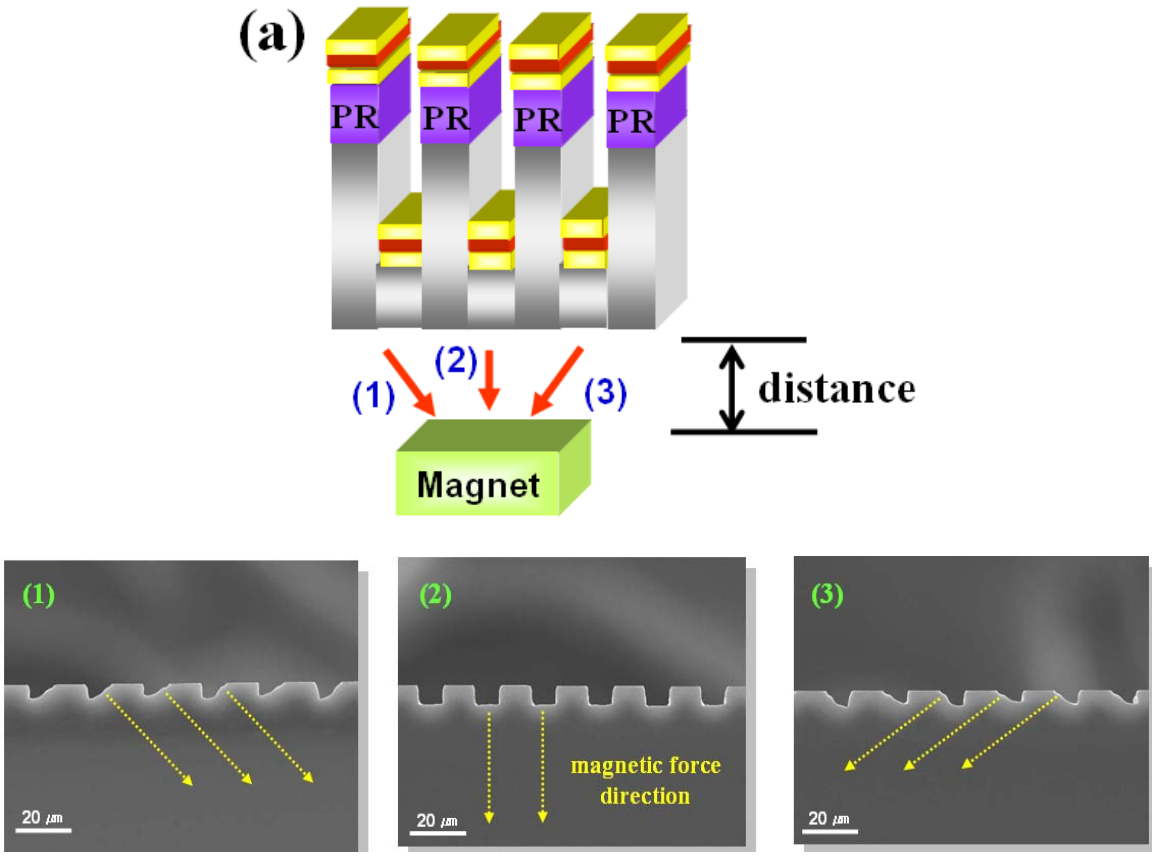

Figure 2-13. (a) Magnetic field directions used. (1), (2), (3) SEM for resultant altered silicon slicing directions.

The magnetically guided Si etching technique can also be utilized for microscale tunneling for unique applications such as microfluidic channel devices, micro fuel cells, and micro combustion channels, for example. Such tunnels do not need to be straight tunnels. Curvatured or zig-zag shaped tunnels may also be drilled by gradually manipulating magnetic field directions in our process {See Fig. 2-14(a) and (b)}. The Au coating on ~1 μm diameter magnetic nanoparticles (oxide or metallic) reacts with the Si and catalytically etches it at the contact interface pulled by magnetic force, thus forming a micro-tunnel. An array of micro-tunnels can be made in parallel by appropriate positioning of the magnetic particles in advance.

By utilizing swiss-cheeze patterned catalyst trilayer deposition (Au/Fe/Au) similarly as for Fig. 2-1, and by altering the magnetic field orientation at specific desired time and at certain desired etched pattern lengths, an abruptly bent or gradually curved Si nanowire array can be obtained as shown in Fig. 2-14(d). A zig-zag Si microwire or nanowire array has also been fabricated as demonstrated in Fig. 2-14(e). The zig-zag bending can be repeated many times by changing the magnetic field direction through repeated movement of a permanent magnet or by selective activation of multi-pole electromagnet.

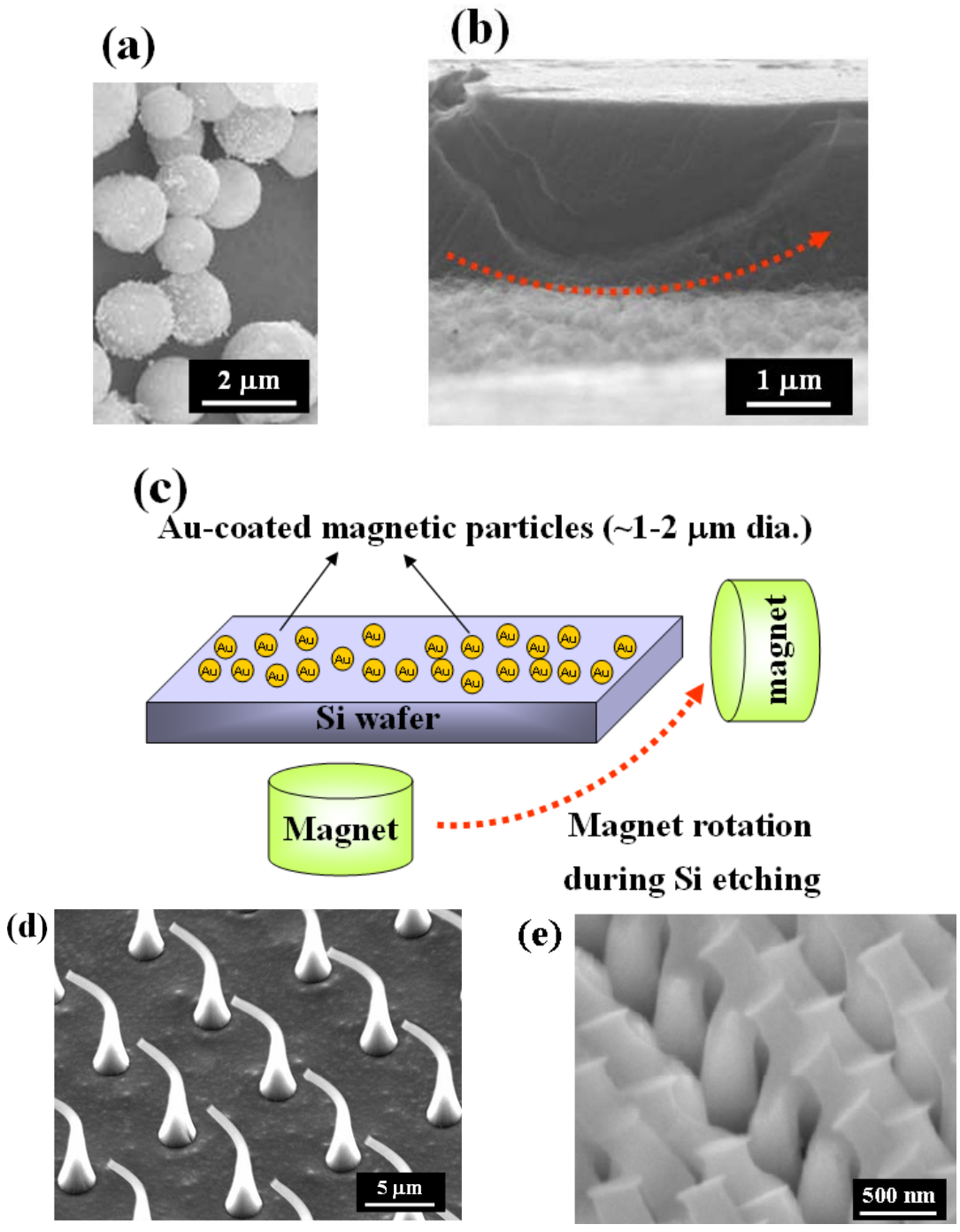

Figure 2-14. Nonconventional Si geometry fabrication. (a) SEM of ferromagnetic microsphere with catalytic Au surface coat, (b) Sectional SEM micrograph showing microscale curved tunnel drilling into Si using magnetically guided etching, (c) Schematics showing the principle of guided tunneling into Si, (d) Example of curved Si microwire array (~700 nm diameter) on large area Si surface, prepared by magnetically guided chemical etch directions, (e) Dense zig-zag-bent Si nanowire array (~300 nm diameter) by magnetic etching.

2.3.2.3 Zig-zag Silicon nanowires for anti-reflective coating

Efficient anti-reflection (AR) coatings are essential for various miniaturized optical sighting systems, enhanced light transmission and imaging, and reduced sunlight loss in solar cells and other energy devices as well as other civilian and military optical system lenses such as for glint-free, stealth movements/operations of soldiers. As the natural light and solar radiation are broadband, the AR coating needs to be effective over a relatively broad light spectrum. The AR coating also has to be effective for all angles of light incidence for many technical applications, as tilted or glazing angle incident light can cause much greater magnitude of light reflection.

Currently available anti-reflection coatings such as the honeycomb-type anti-reflection device (ARD) suffer from the loss of transmission over broad fields-of-view, including the problem of "blue shift", which can cause a loss of critical spectral transmission and lead to unwanted reflections from the front lens or loss of spectral resolution. It has been demonstrated with Si and other materials that an artificially modified surface structure can increase the bandwidth. A periodic sub-wavelength structure (SWS) surface nanostructures such as made with Si, including zig-zag Si nanowires made by GLAD (glancing angle deposition by vacuum evaporation) were shown to suppress reflection in the visible and near-IR. It has been reported that a random silicon nanotip structure can give a total reflectance of less than 1% for wavelength 0.2~2.5 μm. However, the vacuum deposition of nanowires are difficult to scale-up for large-area, large quantity manufacturing. Furthermore, the extreme oblique incident deposition tends to produce coatings with reduced mechanical strength and adhesion.

By contrast, the zig-zag Si nanowires produced by guided magnetic etching (such

as shown as Fig. 2-14(d) and (e) structures and various sub-100 nm diameter structures) according to the this technology are mechanically strong and adherent (since they are still part of the original substrate after etching and shaping), and the process can easily be scaled-up, without costly vacuum deposition equipment required for GLAD type deposition, to larger area substrates and optional multiple aqueous bath productions.

In addition to the sub-wavelength structures as is utilized in nature by moth and butterflies, another way of reducing reflectance for AR coating is to gradually reduce the refractive index of the coating material from that of air at the top to that of the substrate material. Such gradient optical structures are occurring naturally, some examples being the human eye aberration reduction, gradient-index lense structure in the eyes of antelope. The principle of these so called graded refractive index (GRIN) structures is typically explained in terms of density changes in a variable medium, as the reflection is reduced with reduced refractive index cause by density change in porous or nanowired surface.

According to the well-known Cassie-Baxter model, nanowire structures often provide strongly superhydrophobic properties if hydrophobic coating is provided. The bare Si surface typically exhibits hydrophilic characteristics with a contact angle of θ_c ~42 degrees, while the as-magnetically-sliced Si surface is slightly less hydrophilic with θ_c ~80 degrees presumably due to the extremely fine nanoscale surface structures. The as fabricated bent Si or zig-zag Si nanowires of Figure 2-14(d) and (e) are hydrophilic to superhydrophilic. However, with an addition of hydrophobic trichlorosilane coating, the material becomes extremely superhydrophobic as shown in Figure 2-15, with a contact angle of θ_c ~170 degrees for the tall Si microwire array, 161 degrees for 700 nm Si

nanowire array of Figure 2-14(d), and 166 degrees for the zig-zag Si nanowire of Figure 2-14(e), respectively. Such a superhydrophobic behavior of nanowires could be useful for self-cleaning solar cell surface structure (especially in combination with anti-reflective properties) and other non-wettable surface applications.

The anti-reflection property of the magnetic sliced Si wafer is in fact slightly enhanced by the etch process. An addition of bent or zig-zag Si nanowires substantially improve the AR properties as shown in Figure 2-16. Reflectance spectra measurement data (350 – 750 nm range) in Figure 2-16 also shows that the zig-zag Si nanowire array exhibits improved and strong anti-reflection characteristics, with the total reflection significantly reduced to 2~6% regime up to the 650 nm wavelength as compared to the typical ~40% reflection value for the bare Si surface.

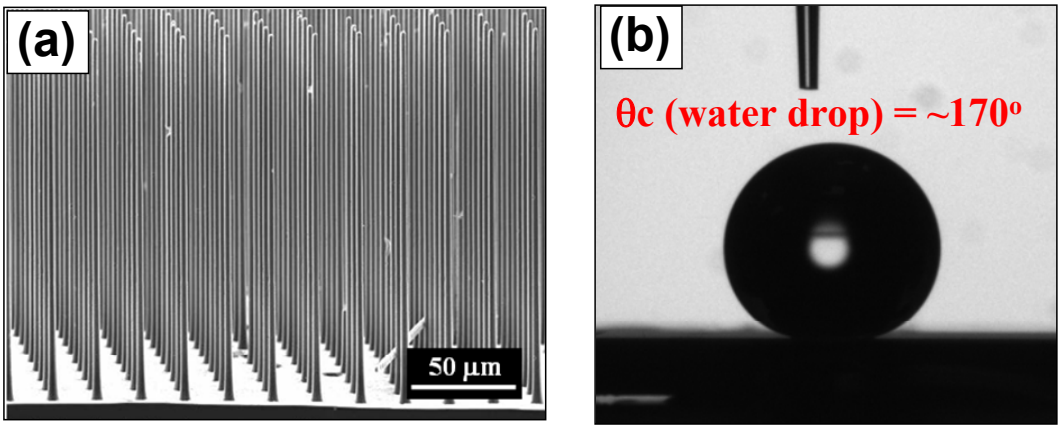

Figure 2-15. (a) Tall Si micropillar array (~1 µm diameter, ~200 µm tall) which is superhydrophilic as made, but becomes strongly superhydrophobic with high water droplet contact angle of θ_c~170 degrees) when a thin coating of hydrophobic trichlorosilane is applied by evaporation.

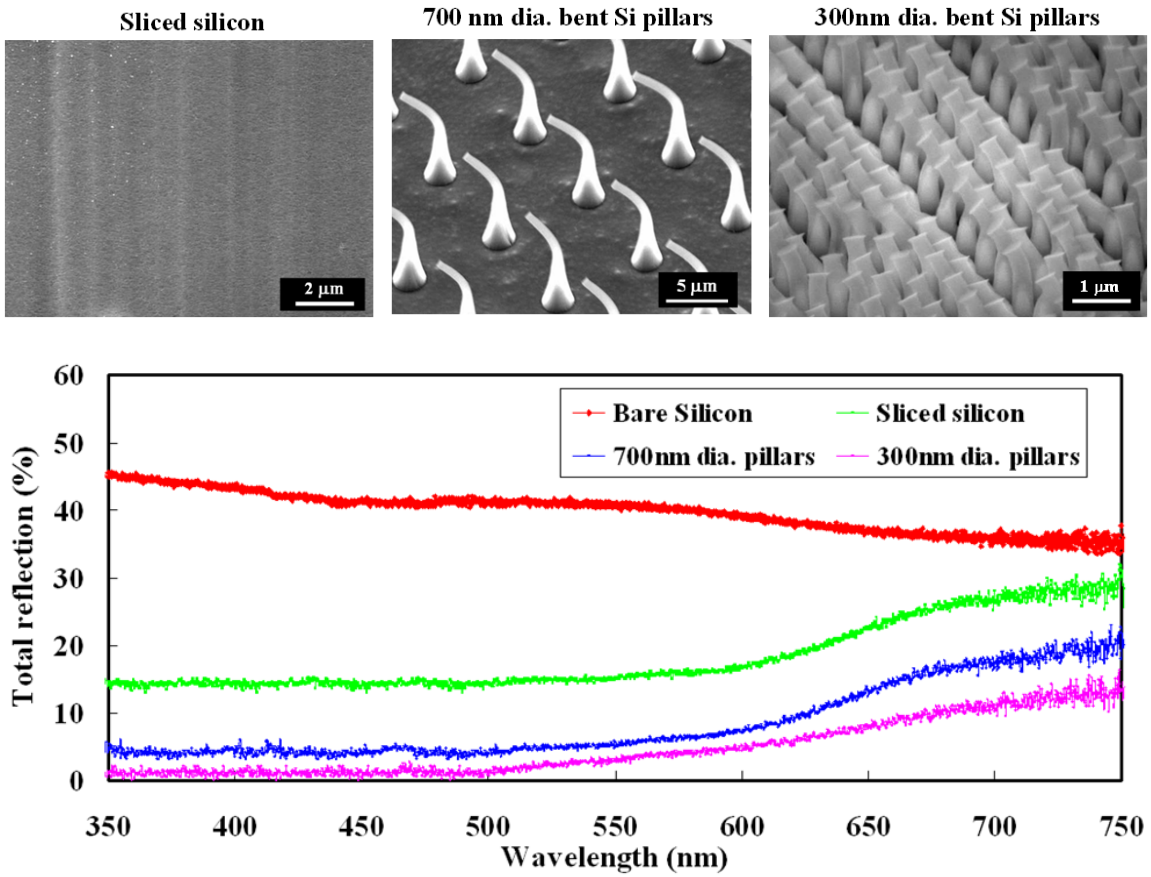

Figure 2-16. Comparative light reflectivity measurements on bare silicon, sliced silicon, 700nm dia. bent Si pillars, and 300nm dia. bent Si pillars.

2.3.2.4 Subwavelength nanostructure arrays

Shown in Fig. 2-17 are schematics of the vertical nanowires with different geometry. Unlike equi-diameter nanowires of Fig. 2-17 (a) which does not produce gradient refractive index, the cone or parabolic-cone structures of Fig. 2-17(b) and (c) possess gradient density and hence exhibits gradient refractive index from that of air to that of the substrate. Shown in Fig. 2-17(d) is an SEM micrograph with ~170 nm diameter Si nanowires beginning to be formed by magnetically guided Si etching. The speed of magnetic etching can be controlled or programmed in a nonlinear fashion using magnetic field strength adjustment so as to produce sharper tips at the top with gradient diameter. An example of gradient diameter Si microwire array is shown in Fig. 2-17(e). Similarly gradient nano-wires can also be obtained. These guided etched structures can be made suitable for anti-reflection coatings for various optical applications, for example, by optional RIE etching to produce further gradient or sharper tips.

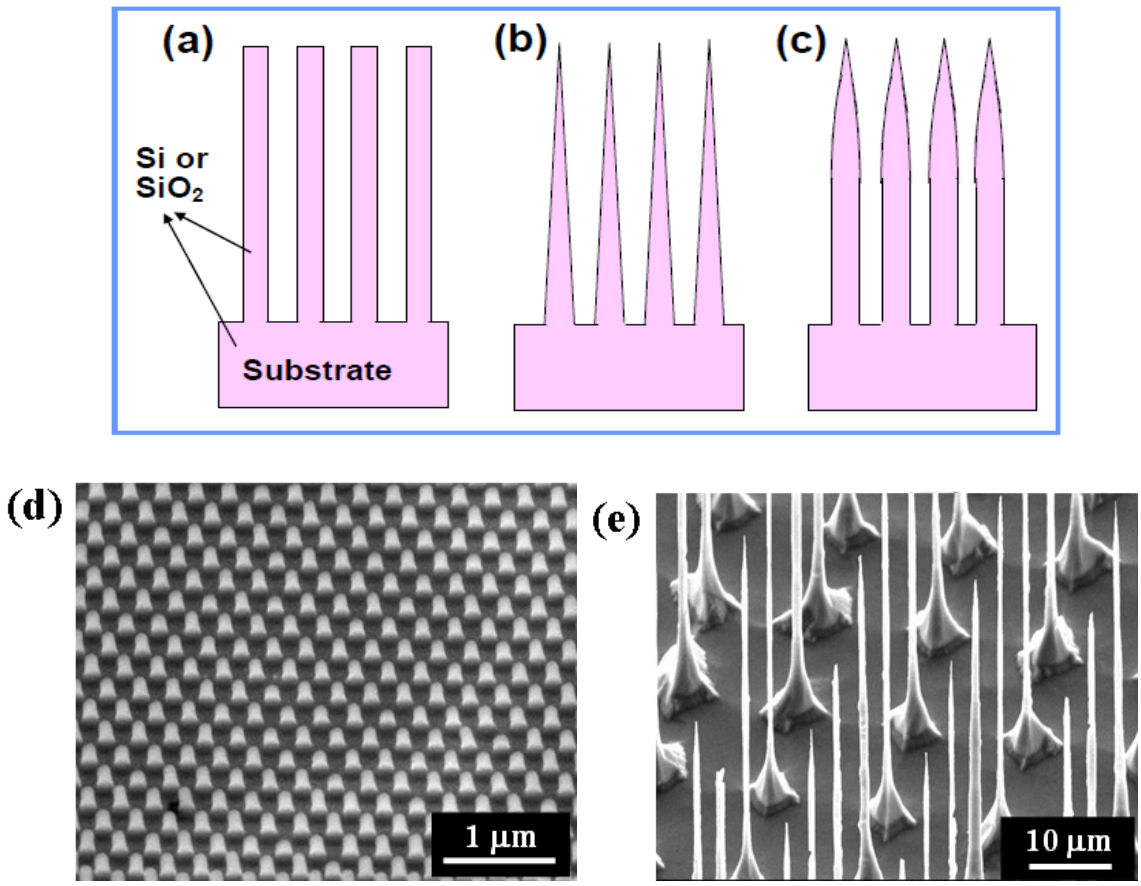

Figure 2-17. Subwavelength nanostructure arrays of Si or SiO_2 nanowires created on the Si substrate surface. (a) Vertical nanowires, (b) Sharp nanocones, (c) Parabolic-tipped nanowires, (d) ~170 nm diameter Si nanowires beginning to be formed by magnetic guided etching. The speed of magnetic etching can be controlled to create sharper tips at the top with gradient diameter. (e) An example gradient diameter Si microwire array.

2.3.2.5 Biotech applications of tall silicon micro-needles

Living cells can be modified by physical science approaches for various purposes. Recently, there has been much interest in cellular injections for drug delivery, gene therapy, and other types of cellular manipulation for drug discovery and research for a deeper understanding of human development and disease. Single-cell transfection has been studied using a commercially available AFM (atomic force microscopy) tip and carbon nanotube tip, but multi-cells transfection using long needle arrays comparable to cell dimensions (e.g., ~50 μm height) has not been seriously investigated. Manual microinjection using a single glass pipette remains the most popular, however other techniques have been developed including viral vectors, electroporation, liposomal carriers, and laser trapping among others. Even though these methods have potential, each of them has short-comings thus making them less attractive for cellular injections. Some of the common disadvantages to these methods are that they often introduce cell damage, loss in viability, increased waste and loss of effectiveness of delivering materials.

One of the advantages of the magnetic-guided Si etching is its ability to fabricate "very tall" high-aspect-ratio Si micro-needles, as tall as ~200 μm tall with only a few μm in diameter as shown in Fig. 2-18. These microneedles are mechanically more compliant due to their small dimension. They can also be coated with an inert metal (Au, Pt) or bioactive metal for enhanced mechanical toughness and easy conjugation and attachment of biomolecules. All metallic micro-needles can also be fabricated using the Si micro-needles as the template. This micro-needle technique provides a new approach for genetic manipulations, by which specific proteins could be synthesized. As the cell commands via signal pathway is affected/decided by specific proteins, the gene delivery into cell

interior using Si micro-needles can be useful. A simple endocytosis of biomolecules to cell interior is not desirable since such endocytosed materials are confined to small membrane-bounded vesicles such as endosomes, and then later moved/sequestered into lysosomes and decomposed by enzymes. Therefore, a direct insertion into the cell cytoplasm or nucleus is often beneficial.

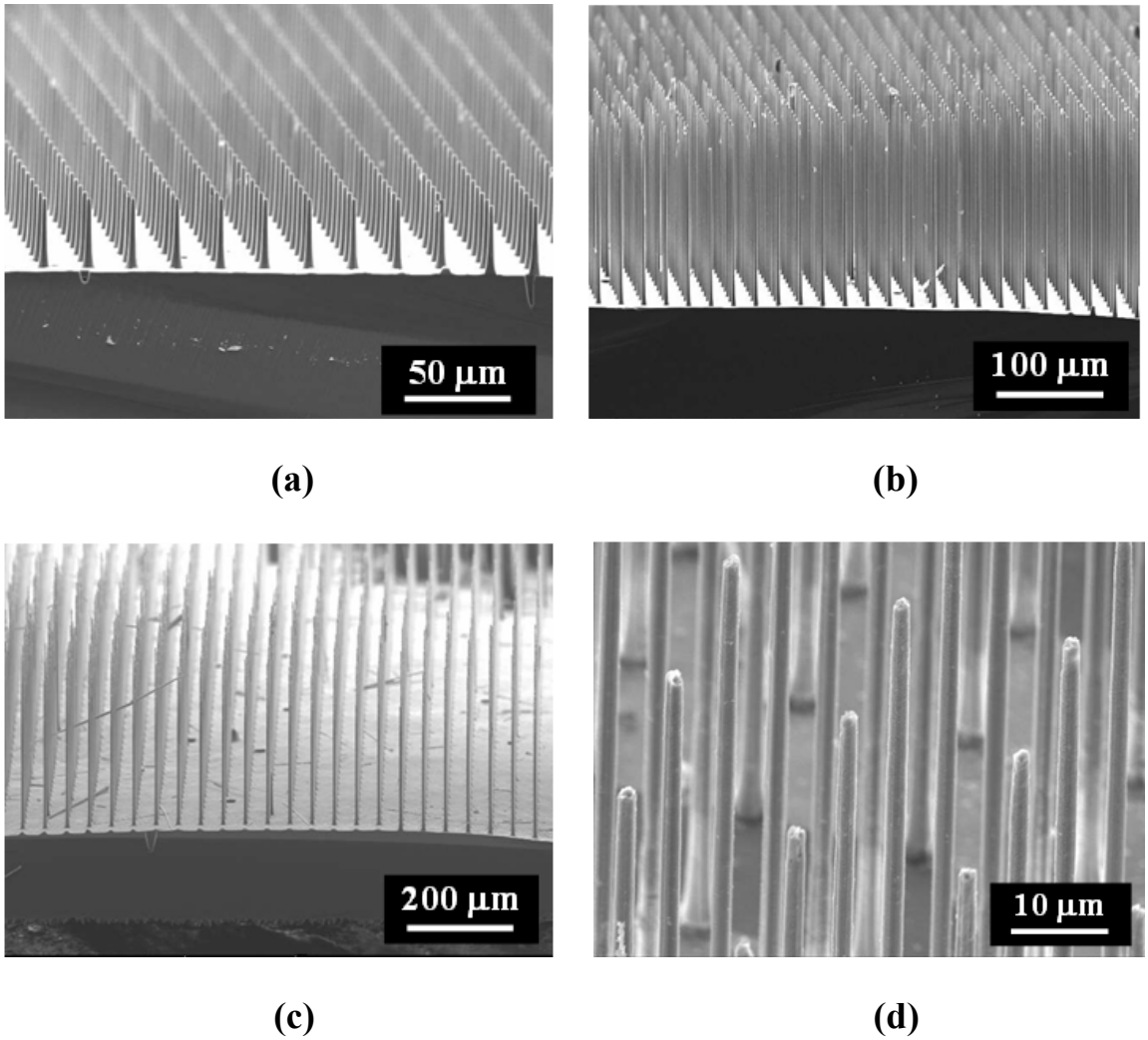

Figure 2-18. Micro pillars produced by magnetic guided etching. (a) height 30 µm, (b) height 150 µm, (c) height 300 µm, (d) enlarged image of Fig 2-17 (c)

As the live cell height is typically 10 - 50 μm, the Si micro-needles to poke into the cells and deliver the biological entity (see Fig. 2-19) need to be tall. The micro-needle diameter needs to be small since the larger the needle size is, the more adverse damages the cells experience. The tip of the microneedles has been sharpened to 30 nm diameter (data not shown), with a gradual change in diameter with the needle height. High-aspect-ratio Si microneedles can be made in large areas, for example, 10 cm x 10 cm area. This area is large enough to contain ~1 million live cells, onto which one can try to insert biomolecules and genetic components to modify these cells simultaneously.

Bio-substances such as various proteins, RNA, DNA, quantum dots, nanoparticles, etc. can be injected by nano/micro-needles for cell therapy protocols, with emphasis on the delivery of nucleic acids, including short interfering RNAs (siRNAs). Normal genes can be i) inserted into the human cells and biological tissue to replace an abnormal disease causing genes (gene therapy) or ii) introduce genes to re-engineer the fate of the cells in the case of stem cells or in the process of creating iPS cells (induced pluripotent stem cells from the patient's own non-pluripotent cells such as skin cells by a forced expression of genes). This type of nano-needle array can be especially beneficial for many cell types including primary cells, neurons, stem cells, and white blood cells, for example.

Some example molecules that can be inserted into cells using the tall Si pillar arrays, according to this technology, are siRNA or fluorescent molecules (such as a green fluorescent protein). As there is a strong need for this type of cell transfection devices, multi-billion dollar business can benefit from the new Si slicing and shaping technology.

As illustrated in Fig. 2-19, the nano-needle array performs the four main functions

necessary in a typical cellular injection device including: i. the adhesion/attraction of payload molecules to the nano-needles, ii. the piercing of the target cells by the nano-needles without cellular damage, iii. release of the payload molecules inside the target cells and iv. the retraction of the nanoneedles from the cells without the loss of viability. One advantage to the tall pillar structure is that one has the added option of using the nano-needle array with the needles pointing upward, to use them as a tissue engineering construct, with the cells growing on top of the needles. The nano-needle array can be utilized for (a) retraction after release or (b) growth of the cells on the needle-array. To test this nano-needle model, basic methods begin with the adsorption of green fluorescent protein (GFP) DNA electrostatically attached on the surface of the nano-needle tip.

Referring to Fig. 2-19(a), specific targeting of the nucleus of human mesenchymal stem cells (MSCs) grown on tissue culture surfaces (in 10% fetal bovine syrum growth media, 5% CO_2 humidified incubator at 37°C) is achieved by using an inverted microscope and x-y-x manipulator to control the positioning. The needle array can remain inserted in the cell nucleus for a few minutes to allow for the diffusion of the DNA from the surface of the needle into the nucleus, then the needles will be extracted.

A second method for using the needle array is shown in Fig. 2-19(b), where the cells are gently forced against the needles. In this manner they can have nucleic acids (DNA/RNA), proteins, or imaging molecules inserted and then the cells are grown on the surface of the array. First, the cells are obtained in a suspension and gently centrifuged downward on top of the needle array. Then, the cells are sandwiched in-between a flat wetted surface and the needle array to gently press the cells so as to penetrate the needles into the cell cytoplasm. Finally, the array is turned with the needles facing upward to

allow for subsequent growth and gene expression. The array serves to provide a mechanical and stimulating support. It is well known that nano-topographical features such as nanorods, nanogrooves, nanotubes, nano-needles have enhanced culture effects on cells.

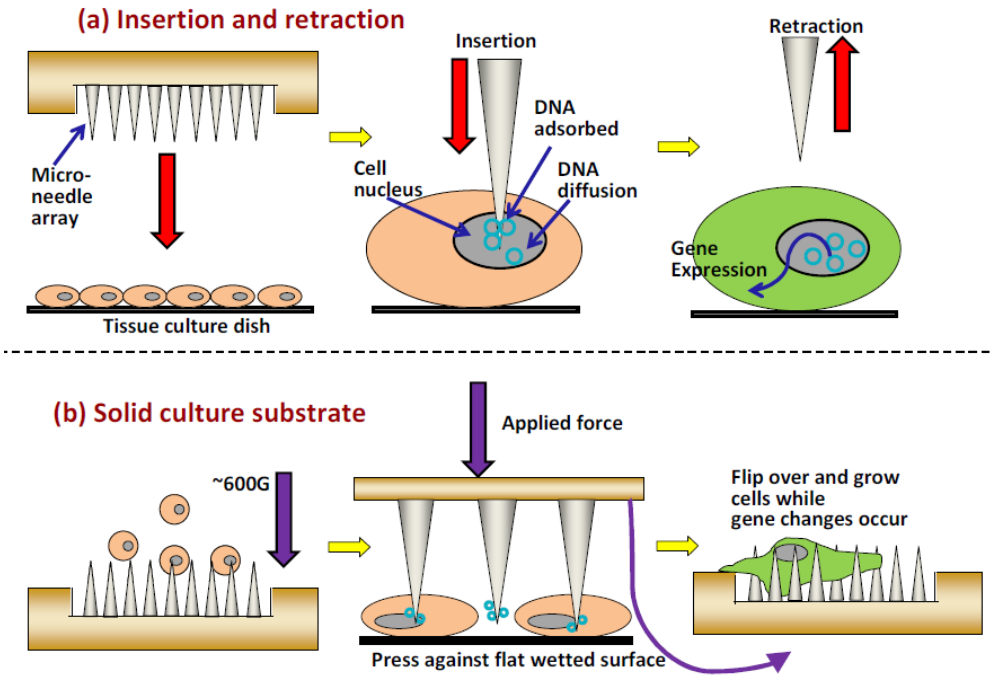

Figure 2-19. Cell poking into multi-cell array using tall Si micro-needles with functionalized tips for delivery of intended biomolecules or other agents for cell modifications.

2.4 Summary

Thousands of parallel micrometer-wide lines of Au/Fe/Au layer deposited on a polymer resist-patterned silicon wafer can simultaneously partition a large area silicon wafer vertically or along any desired angle following the applied magnetic field direction, to produce as thin as ~5 μm thickness wafers. The magnetic material can be either Fe, Co, or CoPt thin film, sandwiched by protective Au thin films. The magnetic gradient interaction of the sandwiched Fe layer with applied field can ensure a straight and vertical slicing at an accelerated rate, while Au surface enables catalytic electroless etching. A modified processing for creation of Zig-zag bent Si microsheet or microwire array is also made possible using changes of magnetic field orientation during etching. A guided micro-tunnel drilling into Si via gradually changing field directions is also demonstrated. Such Si wafer slicing to different orientations or bent/shaped microwires is useful for various new devices utilizing orientation-dependent electronic or photonic properties, or metamaterial aspects.

In addition, a new Si slicing technique with a minimal cut loss of Si during slicing is made possible by constructing a massively parallel etching line arrays (Si micro slicing lines) that can include a magnetic line component sandwiched by catalytic Au line components. Such an arrangement of parallel etch lines enables parallel chemical slicing of silicon ingot into thousands (or tens of thousands) of thin sheets. The slicing speed and direction are guided by the magnetic force direction of externally applied magnetic applied.

2.5 Acknowledgments

This chapter, in full, has been prepared for a manuscript for publication, “Magnetically Guided Nano-Micro Shaping and Slicing of Silicon”, Young Oh, Chulmin Choi, Daehoon Hong, Seongdeok Kong, and Sungho Jin. The dissertation author was the primary investigator and author of this paper.

2.6 References

[1] X. Li and P.W. Bohn, Appl. Phys. Lett. **77**, 2572 (2000).

[2] T. Hadjersi, N. Gabouze, N. Yamamoto, C. Benazzouz, H. Cheraga, Vacuum **80**, 366 (2005).

[3] P. Gorostiza, R. Diaz, M. A. Kulandainathan, F. Sanz, and J. R. Morante, J. Electroanal.Chem. **469**, 48 (1999).

[4] S. Yae, Y. Kawamoto, H. Tanaka, N. Fukumuro, and H. Matsuda, Electrochem. Commun. **5**, 632 (2003).

[5] K. Tsujino and M. Matsumura, Sol. Energy Mater. Sol. Cell **90**, 100 (2006).

[6] J. Zhao, A. Wang, M.A. Green, and F. Ferrazza, Appl. Phys. Lett. **73**, 1991 (1998).

[7] C. L´evy-Cl´ement, S. Lust, S. Bastide, Q.N. L^e, and D. Sarti, Phys. Stat. Sol. A **197**, 27 (2003).

[8] D. S. Y. Hsu and H. F. Gray, Appl. Phys. Lett. **63,** 159 (1993).

[9] V. Lehmann, W. H¨onlein, H. Reisinger, A. Spitzer, H. Wendt, and J. Willer, Thin Solid Films **276**, 138 (1996).

[10] S. Cruz, A. Hönig-d'Orville, and J. Müller, J. Electrochem. Soc. **152**, C418 (2005).

[11] K. Takahashi, H. Terao, Y. Tomita, Y. Yamaji, M. Hoshino, T. Sato, T. Morifuji, M. Sunohara, and M. Bonkohara, Jpn. J. Appl. Phys. **40**, 3032 (2001).

[12] A. Satoh, Jpn. J. Appl. Phys. **40,** 4774 (2001).

[13] S. L. Burkett, X. Qiao, D. Temple, B. Stoner, and G. McGuire, J. Vac. Sci. Technol. B **22**, 248 (2004).

[14] C. L. Lee, K. Tsujino, Y. Kanda, S. Ikeda, and M. Matsumura, J. Mater. Chem. **18**, 1015 (2008).

[15] K. Tsujino and M. Matsumura, Electrochim. Acta. **53**, 28 (2007).

[16] K. Tsujino and M. Matsumura, Adv. Mater. **17**, 1045 (2005).

[17] K. Tsujino and M. Matsumura, Electrochem. Solid-State Lett. **8**, C193 (2005).

[18] W. Lee, H. Han, A. Lotnyk, S. Senz, M. Alexe, D. Hesse, S. Baik, and U. Gosele, Nature Nanotech. **3**, 402–408 (2008).

[19] A. S. M. Chong, L. K. Tan, J. Deng, and H. Gao, Adv. Funct. Mater. **17**, 1629 (2007).

[20] K. Q. Peng, Y. J. Yan, S. P. Gao, and J. Zhu, Adv. Mater. **14**, 1164 (2002).

[21] K. Peng, Y. Wu, H. Fang, X. Zhong, Y. Xu, and J. Zhu, Angew. Chem. Int. Ed. **44,** 2737 (2005).

CHAPTER 3: Multi-tip AFM lithography system for high throughput nano-patterning

This chapter, in full, is a reprint of the material as it appears in Journal of Vacuum Science and Technology B29, 06FD03 (2011), "Multi-tip AFM lithography system for high throughput nano-patterning", Young Oh, Chulmin Choi, Kunbae Noh, Diana Villwock, Gwangmin Kwon, Haiwon Lee, and Sungho Jin. The dissertation author was the primary investigator and author of this paper.

3.1 Introduction

Lithographic techniques based on scanning probe microscopy (SPM) [1] have been applied to nanofabrication processes such as electrical [2] or mechanical deposition or removal of materials [3-5], patterning of magnetic films [6-8], or doping and manipulations [9-12] in science and technical fields. However, SPM lithographic processes have been limited in terms of scale and throughput. In particular, many researchers have made considerable efforts to improve the lithographic speed for high-throughput SPM lithography that meets broad technical demands. Molecules including a highly sensitive functional group have been used to develop electrochemical reactions such as anodization [13,14] and polymerization [15]. High-speed scanner systems related to the movement of a piezo tube scanner also have been developed [16-18]. The traditional AFM lithography based on a single tip probe remains as an inefficient nanopatterning technique with comparatively low throughput.

In order to overcome such limitations, parallel scanning probes have been investigated since the mid 1990's. An array of scanning probes on the base of a piezoresistive cantilever developed by Calvin Quate's research group has demonstrated that large-scale patterning (local oxidation) with a parallel set of cantilevers was possible, and scanning time was reduced compared to patterning the same area with a single probe [19]. Dip-pen nanolithography (DPN) patterning with many AFM cantilevers has been introduced by Chad A. Mirkin's research group to locally transfer patterning or biological materials [20]. The Millipede system composed of high-density thermomechanical AFM cantilever arrays was developed by IBM [21], demonstrating a storage density of more than 1 Tbit/in^2. In addition, a multifunctional probe array for scanning probe contact printing and pattern imaging was developed by Chang Liu's research group [22]. In this chapter, we demonstrate that a multi-tip array on a single AFM cantilever can effectively fabricate multiple structures simultaneously. Such a system avoids the complicated multi-channel multiplexing often required for the multi-cantilever systems. The uniformity and reliability made possible with the proposed multi-tip probe are essential for successful lithographic applications. Such multi-tip AFM lithography may advantageously be used to fabricate high-density data storage media and nano-electronics devices..

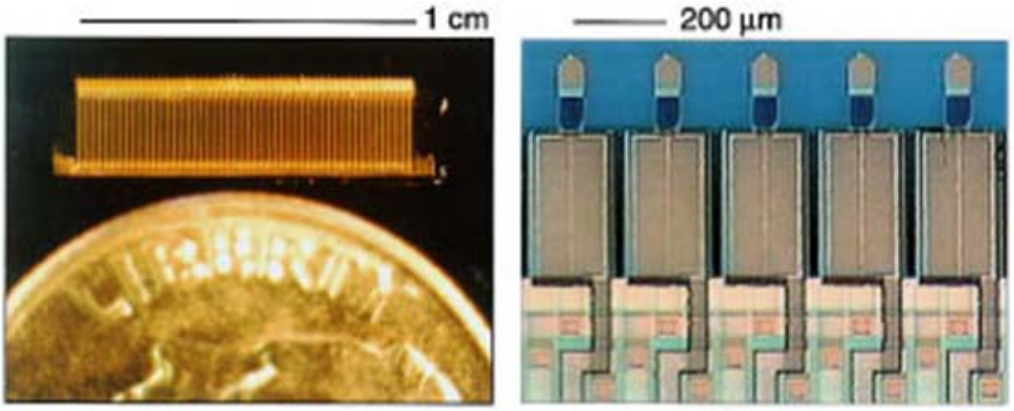

(a)

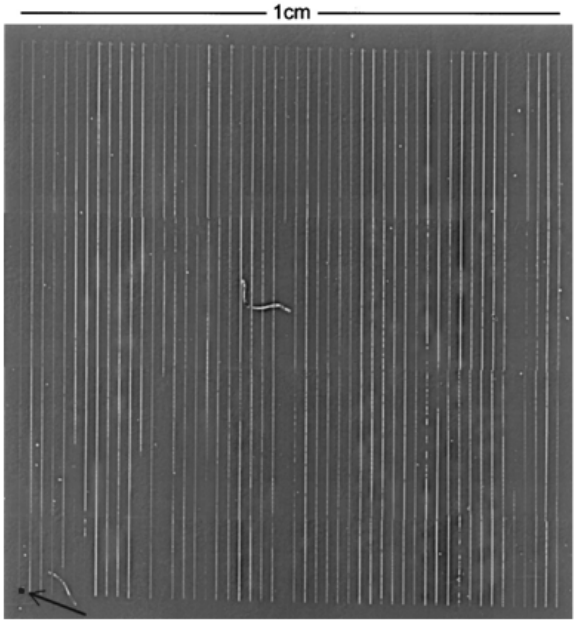

(b)

Figure 3-1. 5031 parallel AFM lithography over 1 cm^2. The lithography was accomplished by electric field enhanced oxidation of silicon at 15 V, and at a scan speed of 1 mm/s. The lithographed oxide pattern was transferred into the silicon using KOH. (a) 50 cantilever, (b) anodized line pattern

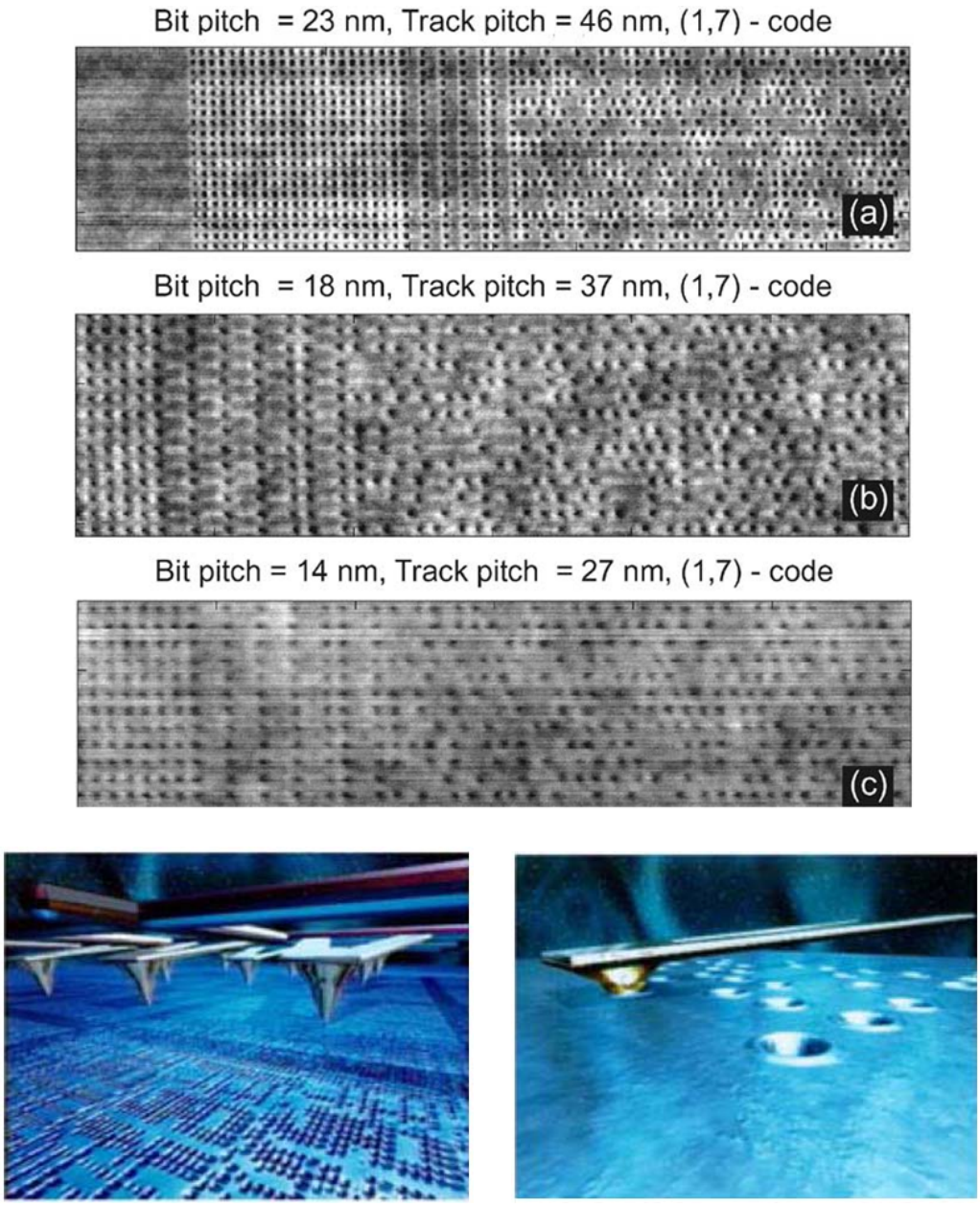

(d)

Figure 3-2. Images of recorded fields at different areal densities. (a) 406 Gbit/in^2, (b) 641 Gbit/in^2, (c) 1.02 Tbit/in^2 In all cases : (1,7) coding is applied in the on-track direction. (d) the schematic of the Millipede system

3.2 Materials and Methods

3.2.1 Multi-tip probes fabrication

A single cantilever (NSC12, Mikromasch Co.) with a low spring constant of 0.65 N/m and a resonant frequency of 41 kHz was used as the base material, and modified for this study. Such a Si-based cantilever has no tip and thus is often referred to as a 'tipless cantilever'. Direct-write e-beam lithography (Raith 50, Raith GmbH) was employed to create carbon dots in parallel on the tipless cantilever at an accelerating voltage of 10kV. Such carbon island formation is based on a well-known EBID (electron beam induced deposition) mechanism which utilizes the decomposition of a residual or injected carbon source in the e-beam chamber. To create pedestal structures and sharpen the tips of the multi-tip probe on a singular cantilever, we used a reactive ion etching (RIE) (Oxford Plasmalab 100) process with the carbon dots as an etch mask. C_4F_8 and SF_6 gases were used to fabricate the tipless cantilevers composed of silicon materials by RIE. The gas flow rates used were 50 and 20 sccm, respectively, at a chamber pressure of 15 mTorr. Additionally, a RIE process with a flow rate of 30 sccm of O_2 gas at a chamber pressure of 90mTorr was run for a few seconds to sharpen the carbon dots located at the top surface of the probe cantilever. Such sharpened carbon dot tips were suitable for high-resolution, multi-tip probe AFM lithography.

3.2.2 Material preparation

The silicon wafer substrates (p-type, boron doped, 100) with resistivities of 1~10 Ω.cm were first cleaned in a 1:3 solution of 30 % H_2O_2 and concentrated H_2SO_4 at room temperature for 1 h, rinsed with de-ionized water for 10 min, and dried under a nitrogen stream. A highly sensitive negative-type e-beam resist terpolymer was applied for the multi-tip AFM lithography experiment. The photo-acid generator (PAG)-containing polymer resist was synthesized by free radical polymerization in tetrahydrofuran (THF) using azobisisobutyronitrile (AIBN). The synthesized poly (MMA64-co-TPSMA36) included 36 % PAG unit to PMMA as a pendant group. This polymer resist was uniformly coated to about 30 nm thickness at a spin speed of 4000 rpm for 30 seconds on a silicon substrate, as shown in Fig. 3-4(a).

3.2.3 AFM lithographic process

In order to induce electron exposure onto a resist film to enhance AFM lithography results, the multi-tip probe was fabricated and mounted on a commercial AFM machine (XE-100, Park Systems Co.). The traditional multi-cantilever parallel scanning probe lithography method requires a multiplexing system for feedback control. Our new AFM does not need such a complicated system, as schematically illustrated in Fig. 3-3. The sharpened carbon tips on silicon pedestals were used for the AFM lithography. DC bias voltage was applied to the sample to induce field emission from the tip to enhance AFM lithography. The substrate sample was attached to the sample holder with conducting colloidal graphite and the sample holder was insulated from the

piezoscanner. The multi-tip AFM lithography, Fig. 3-3, was performed in air at speeds of 1 to 500 μm/sec under a constant force of 37 nN between the tip and the substrate. Also, all experiments were performed in air ambient at room temperature with approximately 60 % relative humidity. A bias voltage of 15 V to 20 V in contact mode was applied to the tip in order to induce the field emission current to enable the local oxidation process [23, 24].

.

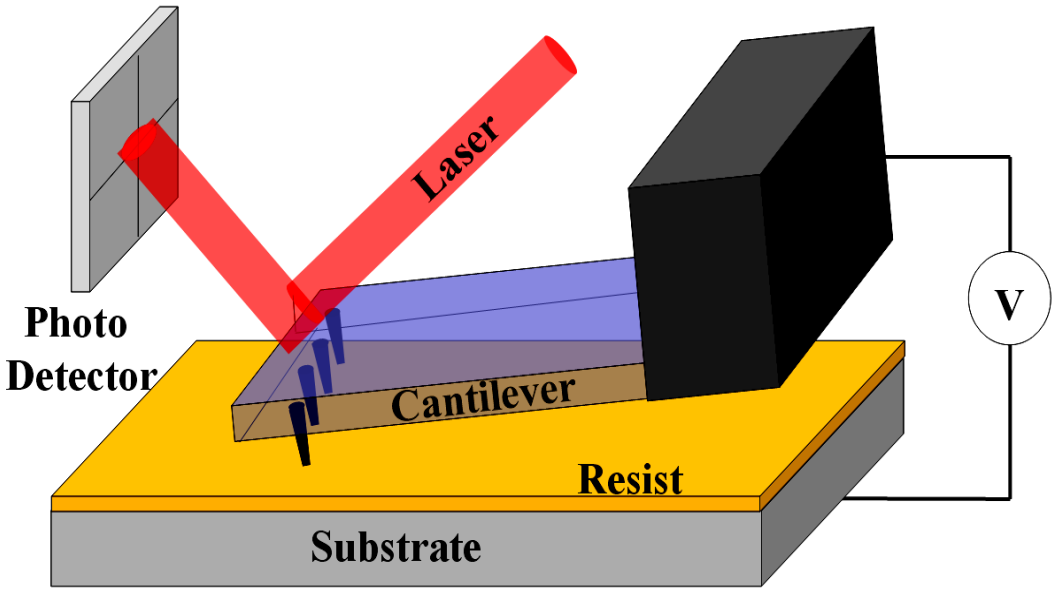

Figure 3-3. Schematic diagram of new AFM multi-tip probe lithography system for pattern writing on a spin-coated resist film

The oxide pattern was generated by applying voltage between the resist-coated silicon sample seen Fig. 3-4(a) and the AFM multi-tip array, as illustrated in Fig. 3-4(b). The primary mechanism of AFM lithography involved in this research is anodization (local oxidation), rather than e-beam lithography. However, local oxidation occurs by field emission from the tip and by the presence of a polymer resist layer, which is used to improve resolution in AFM lithography. Therefore, the final nanoisland structure (~4 nm) is much thinner than the resist (~30 nm) as described in Fig. 3-4(b). The oxidation process can occur without the terpolymer resist, but using a terpolymer layer makes it easier to obtain an anodized nanopattern with a better aspect ratio [25]. After the AFM lithography process, the resist layer was removed by immersion in acetone solution, and the oxidized islands on the silicon substrate were exposed, as seen in Fig. 3-4(c). The structure of the fabricated multi-tip probe on the tipless cantilever was analyzed by field emission scanning electron microscope (SEM) (XL30 ESEM, Philips).

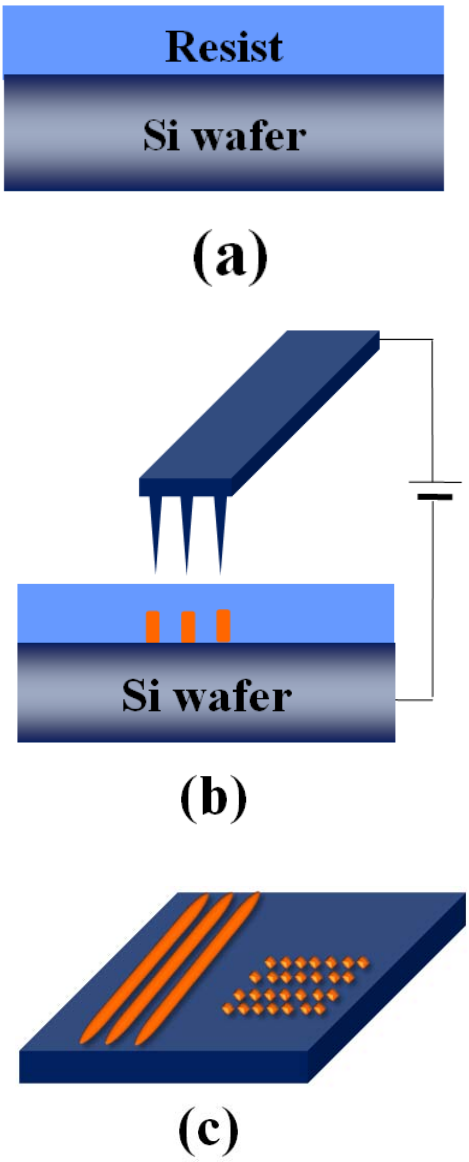

Figure 3-4. Schematic illustration of AFM multi-tip probe lithography procedures: (a) Terpolymer resist spin-coating on a silicon wafer, (b) AFM lithography using a multi-tip probe and applied voltage on a silicon wafer with spin-coated resist film, and (c) resist film removal by a developing solution.

3.3 Results and Discussion

In order to ensure a reliable e-beam exposure from the multi-tip probe system, all tips on a single cantilever should have identical heights and tips with diameters less than 10nm. In contact AFM mode, the distance between a tip and a substrate should be about 0.1~0.2 nm. If the heights of the many write tips on the multi-tip probe are inconsistent, nanopatterning will not be successful. Also, the tip sharpness of the multi-tip probe is a very significant factor for determining the resolution of the final nanopatterned structure.

Figure 3-5(a)-(e) shows a process sequence for the multi-tip fabrication. As a part of the nano-tip fabrication, a linear array of carbon dots was created on a singular AFM tipless cantilever by e-beam lithography process, as illustrated schematically in Fig. 3-5(a). Normally, the resolution of e-beam lithography depends not only on spot size, but on the scattering of accelerating voltage, so we utilized a voltage as low as 10 kV. In addition, we kept the applied current to each tip the same during the EBID process to make multi-tip probes to have an identical tip height. Figure 3-5(d) shows the SEM images of five carbon dots fabricated on a singular cantilever. The diameter and height of the carbon dots are ~ 100 nm and the distance between adjacent tips is 300 nm.

These carbon dots serve two vital functions in our probe tip fabrication.: as an etch mask during the RIE process to produce a pedestal structure underneath the carbon dots; and as the base structure to be sharpened by a subsequent oxygen plasma RIE process for higher resolution multi-tip probe fabrication. Because the tipless cantilever is based on silicon material, a well-defined, vertically oriented Si nano pedestal structure can be fabricated by a silicon RIE process, as illustrated in Fig. 3-5(b). These pedestal

nanopillar structures enable easier control of our multiple nano-tip arrays. The height of each silicon pedestal is adjustable in the range of 0.3 ~ 1 μm depending on the silicon RIE time used. Fig. 3-5(c) shows the final step, in which the top portion of the multi-tip probes was sharpened by an oxygen RIE process. Carbon dots can be rather easily removed by this process it has to be carefully controlled, limiting the carbon dot sharpening time to approximately 20 seconds. Fig. 3-5(e) is a higher magnification image of Fig. 3-5(c). The diameter of the final carbon nano-tip on the Si nanopillar array is very small, estimated to be about 10 nm.

For multi-tip probe parallel lithography operations, we used a very soft cantilever with a low spring constant of 0.65 N/m and a resonant frequency of 41 kHz. A low spring constant is important for reducing the undesirable mechanical stress on the write tips generated by contact force during the lithography process. In contact AFM mode, also known as repulsive mode, an AFM tip makes soft physical contact with the sample. When a stiff cantilever with a larger spring constant was used, the widths and heights of anodized patterns varied significantly each time even with the same setpoint value, and therefore, write experiments were not reproducible. The setpoint is basically a measure of the force applied by the tip to the sample surface to be patterned. In contact mode AFM, the setpoint is related to a certain deflection of the cantilever. This deflection is maintained by the feedback, so that the force between the tip and sample is kept constant. With a low spring constant, the cantilever could naturally adjust to maintain a relatively uniform contact force by all multi-tips on the probe. Such characteristics may somewhat compensate for the geometrical non-parallelness (cantilever width-wise) that may occur during lithography between the probe surface and the substrate surface.

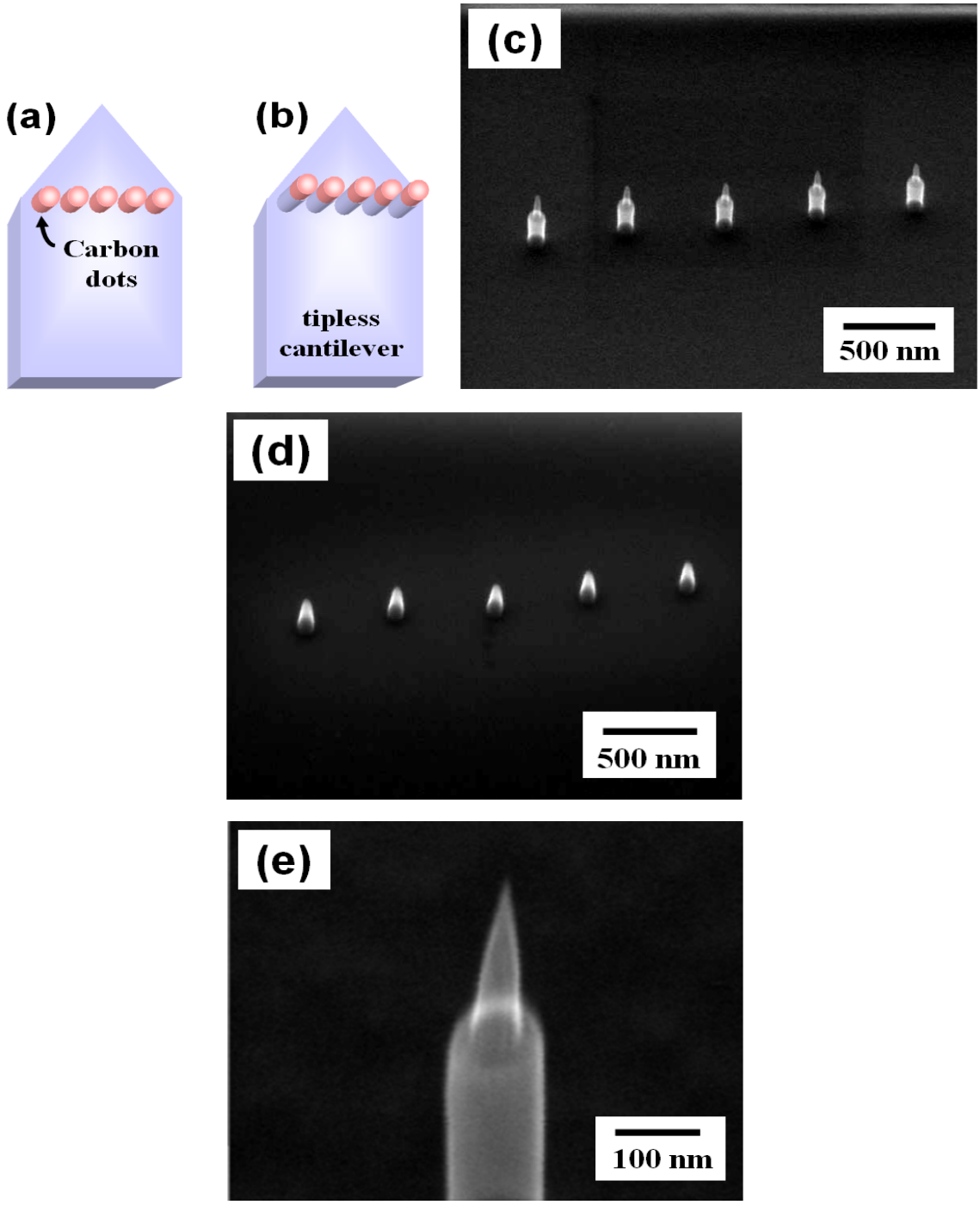

Figure 3-5. Schematic illustration and SEM images of multi-tip probe fabrication procedures: (a) carbon dots created by using an e-beam lithography process, (b) multi-tip pedestal structure fabrication by silicon RIE, (c) SEM image of a five-tip probe with sharp carbon on a single cantilever fabricated by an oxygen RIE method, (d) SEM photography of carbon dots described in Fig. 3(a), and (e) enlarged SEM image of Fig. 3(c) showing sharp carbon tips on a silicon pedestal structure.

Figure 3-6 shows the results of successful AFM lithography nanopatterning conducted using our multi-tip probe. Fig. 3-6(a) shows a schematic illustration of the dot array patterning on a negative resist layer using a three-tip AFM probe on a single cantilever with a low spring constant. The range of setpoint values is 5 ~ 35 nN and the applied voltage is 16 V. Fig. 3-6(b) shows a SEM image of the multi-tip probe positioned on the edge of the tipless cantilever length with 400 nm spacing between each tip. As seen in Fig. 3-6(c), all anodized arrays of three dot patterns exhibit an average diameter of 150 nm and height of 4 nm. The probe performed well on the resist layer on the silicon substrate regardless of various setpoint values.

Figure 3-7(a) shows repetitive array patterns of three dots produced by multi-tip AFM write lithography, which were then imaged by AFM metrology analysis. The applied sample vias voltage is 16 V and the setpoint value is 20 nN. The distance between each tip is 400nm and tip height is 400 nm, as shown in Fig. 3-7(b). Overall, all anodized dots are uniform in height, diameter, and dot-to-dot distance. The ability to control the shape of the multi-tip probe under a variety of experimental process conditions was extremely promising. Another positive finding was that the surface of the resist film clearly plays an important role as a soft bumper maintaining electrochemical contact between the tip and the substrate.

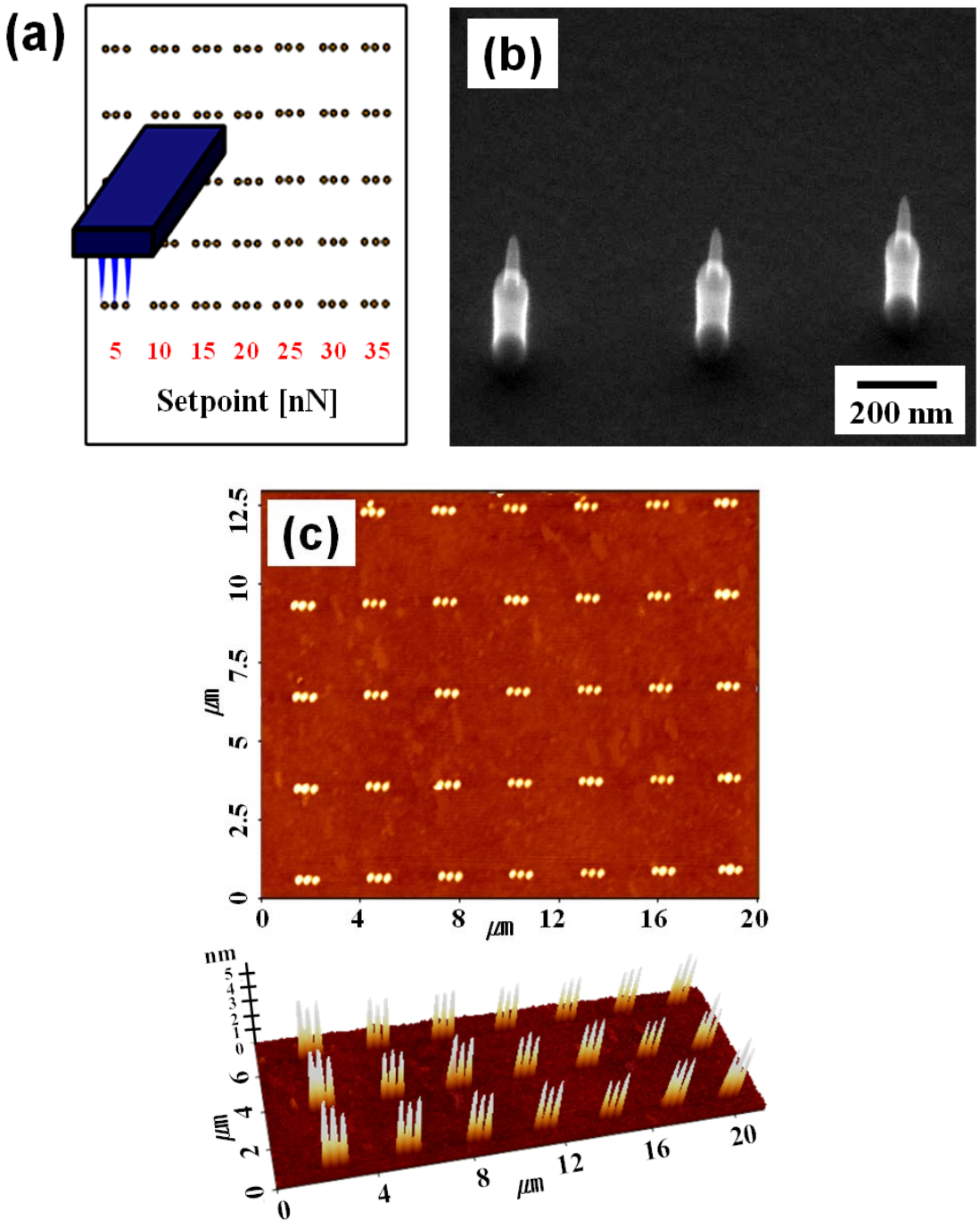

Figure 3-6. Dot array pattern created by multi-tip AFM probe exposure with various setpoint values (5 ~ 35 nN): (a) schematic design regarding setpoint values, (b) SEM image of a three-tip probe on a single AFM cantilever, (c) AFM topographic image of periodically anodized three-dot array pattern.

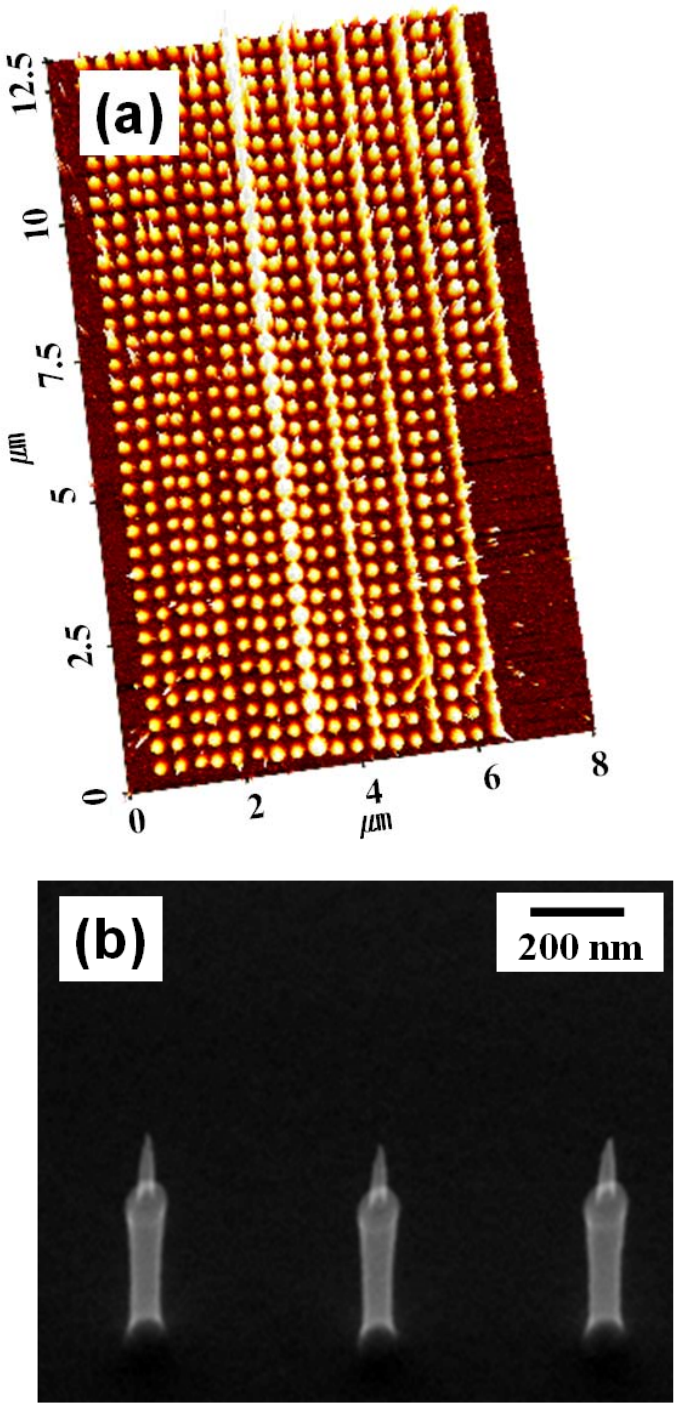

Figure 3-7. (a) AFM topographic image of anodized dots sequentially fabricated by the multi-tip probe of Fig. 5(b); (b) SEM photograph of the three-tip probe.

Figure 3-8 shows that a four-dot repetitive pattern was successfully imprinted by the four AFM multi-tips on the cantilever. The dots had an average diameter of 120 nm and height of 4 nm. Over 2000 dot patterns were uniformly fabricated at an applied voltage of 15 V and a setpoint of 20 nN. The multi-tip probe was moved laterally to create the letters "TND", as shown in Fig. 3-8(a). The multi-tip probe was moved around stepwise to write a series of patterns over a larger area. We have also successfully demonstrated a multiple parallel line lithography (instead of a dot pattern lithography) using the same device but a different mode of operation (data not shown).

The eventual goal is to produce many thousands of tips on the same cantilever (either an AFM pedestal or a larger scale MEMS cantilever) for simultaneous, very large scale parallel writing. Again, the multi-tip probe system does not need to have a multiplexing system for individual feedback and control of each cantilever since a single cantilever can easily produce a multiple and periodic island array pattern or a specific pre-programmed array configuration. Such a multi-tip AFM lithography technique can be used to fabricate high-density data storage technology such as patterned magnetic recording media for hard disk memory, nano-photonics, and nano-electronics devices. Because the multi-tip density and spacing can be adjusted, and the generated pattern configurations and dimensions can be altered via AFM writer movement control, this new lithography method can also be utilized to produce a variety of devices with either periodic or design-specific nanopattern arrays.

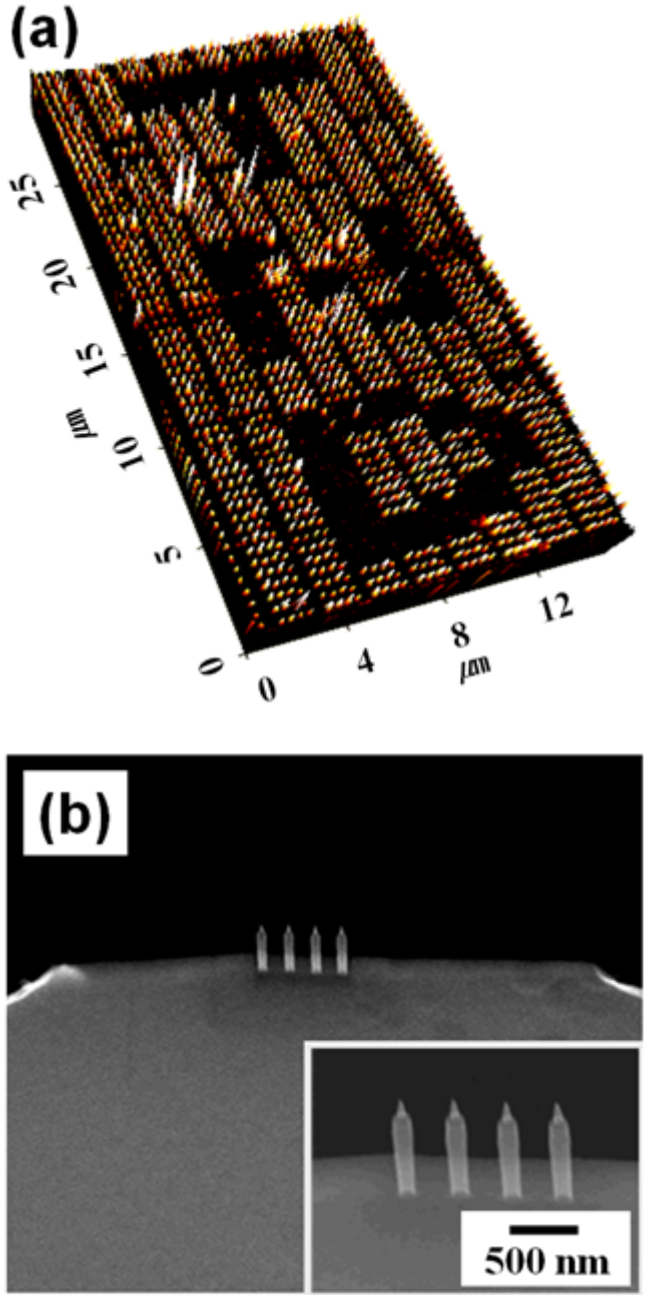

Figure 3-8. (a) AFM topographic image of the letters "TND" written by multi-tip probe lithography; (b) SEM photograph of a four-tip probe located at the end of a single cantilever. The insert is an enlarged SEM picture of the multi-tip probe.

Comparing our multi-tip, single cantilever approach with the multi-cantilever AFM devices, the latter offers an advantage in terms of maximum accessible area and stitching. However, the multi-tip, single cantilever device can be made on a larger scale so as to enable nano-patterning of substrates with larger areas. For example, we have prepared a multi-tip silicon substrate of 0.6 cm x 0.6 cm area with 100 million tips of essentially identical heights. Tips were sharpened to a diameter of less than 10 nm, using a process similar to that used in this study. This approach can also be expanded to an even larger area substrate (unpublished work). Such nanoprobe array results and nanopatterning data will be summarized in future publications. The durability and reliability of the AFM multi-tips are important aspects for long-term applications. The mechanical durability of our multi-tips needs to be better understood for potential reliable applications. Such aspects will be our focus in future studies.

3.4 Summary

In summary, we conducted research on multi-tip, single-cantilever AFM lithography using a probe cantilever nanofabricated by an etching process using a carbon island array mask. The AFM lithography process under low electric field was successfully applied to form multi-dot patterned arrays and multi-line structures on a Si wafer. Also, we used a soft tipless cantilever with a low spring constant to improve the contacts between the multi-probe and substrate. Reactive ion etching process parameters were adjusted to form the multi-tip probe with a regime of sub-10 nm tip sharpness. Such multi-tip AFM lithography has applications for fabricating high-density data storage technology, nano-photonics, and nano-electronics devices.

3.5 Acknowledgments

This chapter, in full, is a reprint of the material as it appears in Journal of Vacuum Science and Technology B 29, 06FD03 (2011), "Multi-tip AFM lithography system for high throughput nano-patterning", Young Oh, Chulmin Choi, Kunbae Noh, Diana Villwock, Gwangmin Kwon, Haiwon Lee, and Sungho Jin. The dissertation author was the primary investigator and author of this paper.

3.6 References

[1] R. Garcia, R. Martinez, and J. Martinez, Chem. Soc. Rev. **35**, 29 (2006).

[2] S. Hong, J. Zhu, and C. A. Mirkin, Science **286**, 523 (1999).

[3] G. Liu, S. Xu, and Y. Qian, Acc. Chem. Res. **33**, 457 (2000).

[4] S. Kramer, R. R. Fuierer, and C. B. Gorman, Chem. Rev. **103**, 4367 (2003).

[5] D. Pires, J. L. Hedrick, A. D. Silva, J. Frommer, B. Gotsmann, H. Wolf, M. Despont, U. Duerig, and A. W. Knoll, Science 328, 732 (2010).

[6] R. W. Li, T. Kanki, and H. A. Tohyama, J. Appl. Phys. **95**, 7091 (2004).

[7] M. Hirooka, H. Tanaka, R. Li, and T. Kawaia, Appl. Phys. Lett. **85**, 1811 (2004).

[8] R. W. Li, T. Kanki, H. A. Tohyama, M. Hirooka, H. Tanaka, and T. Kawai, Nanotechnology **16**, 28 (2005).

[9] R. H. Kim, W. S. Ahn, S. H. Han, and S. K. Choi, Appl. Phys. Lett. **90**, 172907 (2007)

.

[10] R. W. Li, T. Kanki, M. Hirooka, A. Takagi, T. Matsumoto, H. Tanaka, and T. Kawai, Appl. Phys. Lett. **84**, 2670 (2004).

[11] L. Pellegrino, E. Bellingeri, A. S. Siri, and D. Marré, Appl. Phys. Lett. **87**, 064102 (2005).

[12] K. F. Braun and K. H. Rieder, Phys. Rev. Lett. **88**, 096801 (2002).

[13] G. Kwun, E. Jang, G. Kwon, and H. Lee, Current Applied Physics **9**, S121 (2009).

[14] W. Lee, H. Lee, and M. Chun, Langmuir **21**, 8839 (2005).

[15] E. Jang, G. Kwun, W. Choi, and H. Lee, Colloids Surf. A: Physicochem. Eng. Aspects **382**, 313 (2008).

[16] G. Kwon, S. Kim, M. Jeong, S. Han, C. Choi, S. Han, J. Hong, and H. Lee, Ultramicroscopy **109**, 1052 (2009).

[17] D. Croft, G. Shed, and S. Devasia, J. Dyn, Syst. Meas. Control **123**, 35 (2001).

[18] L. M. Picco, L. Bozec, A. Ulcinas, D. J. Engledew, M. Antognozzi, M. A. Horton, and M. J. Miles, Nanotechnology **18**, 044030 (2007).

[19] S. C. Minne, J. D. Adams, G. Yaralioglu, S. R. Manalis, A. Atalar, and C. F. Quate, Appl. Phys. Lett. **73**, 1742 (1998).

[20] K. Salaita, Y. Wang, R. A. Vega, and C. A. Mirkin, Nature Nanotechnology **2**, 145 (2007).

[21] H. Pozidis, W. Haberle, D. Wiesmann, U. Drechsler, M. Despont, T. R. Albrecht, and E. Eleftheriou, IEEE Trans. Magn. **40**, 2531 (2004).

[22] X. Wang and C. Liu, Nano letters **5**, 1877 (2005).

[23] J. A. Dagata, Science **270**, 1625 (1995).

[24] C. Martin, G. Rius, X. Borrise, and F. Perez-Murano, Nanotechnology **16**, 1016 (2005).

[25] N. S. Losiilla, J. Martinez, and R. Garcia, Nanotechnology **20**, 475304 (2009).

CHAPTER 4: Conclusions and Future Directions

Silicon is one of the most important materials for modern electronics, telecom and photovoltaic (PV) solar cells. With the rapidly expanding use of Si in the global economy, it would be highly desirable to reduce the overall use of Si material, especially to make the PVs more affordable and widely used as renewable energy source. Here we report first successful direction-guided, micro/nano shaping of silicon, the intended direction of which is dictated by applied magnetic field. Micrometer thin, massively parallel silicon sheets, very tall Si microneedles, zig-zag bent Si nanowires, and tunnel-drilling into Si substrates have all been demonstrated. Such a convenient Si slicing with minimal loss of Si material waste (as little as ~5 μm thickness of Si wasted per each wafer cut, as compared to the current wire saw cut with ~200 μm cutting loss thickness) has significant implications, as the drastically reduced cost for single crystalline (or polycrystalline) Si wafer would make the crystalline Si photovoltaics much more cost competitive as compared to other renewable or fossil fuel energy sources. Such a convenient and manufacturable Si slicing with minimal loss of Si material (only ~5 μm thickness of Si wasted per cut) could have significant implications for enabling practical photovoltaics applications. Furthermore, the ability for massively parallel cutting to produce thin Si wafers as thin as 5 ~ 20 μm offers an additional significant advantage of using thinner wafers for even lower cost PV solar cells. Another important aspect to consider is the Si feedstock materials availability issue in that the overall Si materials consumption in PV solar cell industry, as well as in the semiconductor electronic device industry, could also be reduced significantly by utilizing thin wafer solar cells. We expect that such

nano/micro-shaping will enable a whole new family of novel Si geometries and exciting applications including flexible Si circuits, biological cell modifications and highly anti-reflective zig-zag nanowire coatings.

Secondly, an atomic force microscopy (AFM) system with multiple parallel lithography probes of equal heights on a single cantilever was created in order to improve the throughput of AFM lithography. The multi-tip probe was fabricated by e-beam lithography and a dry silicon etching process. Several carbon islands were made on a single cantilever in a straight line by e-beam lithography and were used as an etch mask while the silicon pedestal structure of the multi-tip probe was fabricated by reactive ion etching (RIE). Finally the carbon islands were sharpened by a RIE process using oxygen gas. The multi-tip probe was successfully applied to form multi-dot pattern arrays on a negative resist film coated on silicon by low electric field induced AFM lithography. Pedestal nanopillar structure was utilized as a convenient support feature that enabled better control of multiple nanotip arrays for AFM writing. We fabricated such a nano-pedestal array with extremely sharp nano needle tips. In future, if we have the way to make 100 million probe tips with identical height on the cantilever, 100 million identical devices will be fabricated at the same time and we can also create 1~10 Terabit/in^2 density patterned media or custom nano-patterning of nano-electronic devices, memory devices (magnetic, charge-storage, SET, QBit, etc), nano-photonics (QD arrays).